Variational approach for nonsmooth elasto-plastic dynamics with contact and impacts

Vincent Acary, Franck Bourrier, Benoit Viano

Variational approach for nonsmooth elasto-plastic dynamics with contact and impacts

Vincent Acary*, Franck Bourrier*,†, Benoit Viano*

February 8, 2023

Abstract The objective of this article is the modelling and the numerical simulation of the response of elastoplastic structures to impacts. To this end, a numerical method is proposed that takes into account one-sided contact (Signorini condition) and impact phenomena together with plasticity in a monolithic solver, while accounting for the non-smooth character of the dynamics. The formulation of the plasticity and the contact laws are based on inclusions into normal cone of convex sets, or equivalently, variational inequalities following the pioneering work of Jean Jacques Moreau (1974) and Halphen and Son Nguyen (1975), who introduced the assumptions of normal dissipation and of generalised standard materials (GSM) in the framework of associated plasticity with strain hardening. The proposed time–stepping method is an extension of the Jean and J. J. Moreau (1987) scheme for nonsmooth dynamics. The discrete energy balance shows that spurious numerical damping can be removed and the scheme is practically unconditionally stable. Furthermore, the finite-dimensional variational inequality at each time–step is well-posed, can be solved by optimisation methods for convex quadratic programs, providing an interesting alternative to the return mapping algorithm. The paper is completed by numerical illustrative examples of impacts on metallic structures made of beams.

Keywords: contact, impact, plasticity, nonsmooth dynamics, variational inequality, normal cone, generalised standard materials, saddle point, time–stepping methods, numerical optimisation.

Highlights.

1. A formulation of all the dynamical equations of the elastoplastic law and contact law in a single variational inequality, respecting the principles of the thermodynamics
2. A time–stepping method, on the basis of the Moreau-Jean time stepping scheme is developped enabling the integration of the nonsmooth dynamics consistently with the impulsive motion.
3. Formulation of a convex quadratic program with well-posedness results (existence and uniqueness) that can be solved efficiently with large time/load increment. This ensures that the scheme is well-posed
4. A discrete energy balance is given that ensures that the scheme is practically stable.
5. Simulation of multi-criteria elasto-plastic flow rules with contact constraints. Application to impact on structures made of beams.

*Univ. Grenoble Alpes, Inria, CNRS, Grenoble INP, Institute of Engineering, LJK, 38000, Grenoble
†Univ. Grenoble Alpes, INRAE, ETNA, 38000, Grenoble, France

Notation The notation used are quite classical and are not defined in an exhaustive way. We follow the notation introduced in the standard textbooks. For vector and tensors, we choose the following notation:

$$\|\boldsymbol{x}\|^2 = \|x\|^2 = \underbrace{x_i x^i}_{\text{indicial notation}} = \underbrace{\boldsymbol{x}.\boldsymbol{x}}_{\text{tensor notation}} = \underbrace{x^\top x}_{\text{vector notation}} \tag{1}$$

The set T_s^d is the set of symmetric tensors of order s in dimension d. For a convex set $C \subset \mathbb{R}^n$, the normal cone to C at x is defined by

$$N_C(x) = \{s \in \mathbb{R}^n \mid s^\top (y - x) \leq 0, \text{ for all } y \in C\}. \tag{2}$$

For a convex function φ, its subdifferential is denoted by $\partial\varphi$. The indicator function of C is denoted i_C and we have $N_C = \partial \mathrm{i}_C$. For a function $F : \mathbb{R}^n \to \mathbb{R}^n$, the inclusion

$$-F(x) \in N_C(x) \text{ or equivalently, } F^\top(x)(x - y) \geq 0, \text{ for all } y \in C \tag{3}$$

defines a (finite dimensional) variational inequality.

1 Introduction

The impact on elastoplastic solids and structures is an important research topic due to its numerous applications. In solid mechanics, the modelling of impact and plasticity phenomena is required for the reliability of metallic mechanical parts to impacts or in shot peening processes (Levers and Prior, 1998; Majzoobi et al., 2005; Nouguier-Lehon et al., 2013), for example. Generally, impacts, even at low speed, generate plastic deformations, possibly localised in the materials (Johnson, 1985), which can have strong consequences on their dimensioning. Examples include civil engineering applications such as vehicle impacts on buildings and structures (L. Chen et al., 2021; K. Heng et al., 2022; P. Heng et al., 2016, 2017), or ship impacts on harbour infrastructure (Guo et al., 2020; Sha et al., 2021). In the field of natural hazard mitigation, many applications require the joint modeling and simulation of plasticity and impact. Among them, we can cite building pounding (Langlade et al., 2021), the impact with soil foundation during earthquakes, the impact of rock blocks in the mountains against protective structures (walls, nets, or trees)(Bertrand et al., 2012; Di Giacinto et al., 2020; Dupire et al., 2016a,b), and finally impacts on rail, road or electrical transport infrastructures (Kaewunruen et al., 2018; Zeng et al., 2018).

The objective of this article is the modelling and the numerical simulation of the response of elastoplastic structures to impacts. To this end, a numerical method is proposed that takes into account one-sided contact (Signorini condition) and impact phenomena together with plasticity in a monolithic solver, while accounting for the non-smooth character of the dynamics. Furthermore, the goal is to ensure that the method is stable by formulating a discrete energy balance and yields an optimisation problem that is well-posed at each time step.

The numerical solution of elastoplasticity problems is generally based on the return mapping method, attributed to Wilkins (1963) and detailed in the Simo and Hughes (1998) uncontested book. This method is very efficient and robust in many cases provided that the initial iterate is sufficiently close to the solution (see Scherzinger (2017) for recent advances). The local quadratic convergence is a major asset of the method, but it requires a rigorous work of construction and development of consistent tangent operators, which contain conditional statements that are difficult to deal with. Furthermore, as it is noted in Zheng et al. (2020), convergence of the return mapping algorithm is only local, meaning that we need to start from a good initial point preventing large load increments. Some globalisation methods exist, but they generally required a potential to minimize. In Christensen (2002b), it is shown that this method is a special case, for particular parameter choices, of a semismooth Newton method applied to a projection-based reformulation of the variational inequality that describes plasticity (Son, 1977). A similar approach is followed in Bruno et al. (2020) using conic optimization. One of the ideas of the proposed contribution is to return to the basis of the plasticity formulation, as variational principles, and to incorporate contact and impact conditions. In doing so, we will also be able to take advantage of a large set of numerical methods, coming from optimisation and mathematical programming.

The formulation of the plastic flow in solids as a variational inequality is not new, and well known. The really interesting point is that it allows, in some cases, convex analysis and mathematical programming to design efficient algorithms. R. Hill (1948) proposed a variational formulation for the plasticity problem in the case of perfect plasticity from the principle of maximum plastic work (also detailed in Rodney Hill (1950)). Giulio Maier (1968a,b, 1969), with its coworkers in Michele Capurso and Giulio Maier (1970), first considered this principle in their works from the end of the 60's, writing the constitutive laws formulation as a mathematical problem which leads also to a variational formulation.

The formulation as a mathematical programming problem, more precisely of complementarity type, and the maximum dissipation principle problem are the two sides of the same coin. J. J. Moreau (1970, 1971, 1976) and Jean Jacques Moreau (1974), one the father of convex analysis, recognised this structure of the problem as an inclusion in a normal cone to a convex set. Extending the works of Ziegler (1958, 1962) on normality for nonsmooth potentials, he postulated the existence of a pseudo-potential of dissipation given by a lower semi-continuous convex function. With the normality rule and the convexity of the yield criterion, the constitutive equations of plasticity are formulated as a variational inequality, or equivalently, a normal cone inclusion into a convex set. With the notion of subdifferential, the principle can easily be extended to non-smooth yield surfaces described by multiple yield criteria. A recent account on this subject can be found in Guy T. Houlsby (2019).

Following this pioneering research, Halphen and Son Nguyen (1975) introduced the notion of generalised standard materials (GSM). The plasticity law with internal variables follows the normality rule between the plastic strain rate and the yield surface, by assuming pseudo-potential of dissipation. Gery De Saxcé (1992) introduced the notions of bi-potential function and implicit standard materials, that extend the framework to non-associated plasticity (see Cheng et al. (2015) for a recent application of the method). From J. J. Moreau (1970), Halphen and Son Nguyen (1975) to Gery De Saxcé (1992), this approach based on convex and variational analysis generated many contributions and is nowadays called the nonsmooth mechanics framework.

Once the continuous problem is formulated in the nonsmooth mechanics framework, the discretization in space, and possibly in time, leads to problems of finite-dimensional variational inequalities and complementarity problems (Facchinei and Pang, 2003). With some further assumptions such as the normality rule and the convexity of admissible sets, these problems can be recast into optimisation problems. The main advantage of this approach is that it makes it possible to use a wide range of numerical methods developed in the optimisation and mathematical programming community, which are robust, experienced and with global convergence (Boyd and Vandenberghe, 2004).

As we previously explained, pioneering works that extensively used the mathematical programming tools are those of Maier and co-workers: study of reinforced concrete beams (Donato and G. Maier (1972), Leone Corradi, De Donato, et al. (1974)), developing limit analysis (L. Corradi (1976), Giulio Maier and Leone Corradi (1974), M. Capurso (1975), G. Maier and Vitiello (1974) and review in Leone Corradi and Nova (1974)), application and study of programming methods (Donato and G. Maier (1972), L. Corradi (1976), De Donato and Franchi (1973)). Most of these work are in the quasi-statics setting except (L. Corradi, 1976; Leone Corradi and Nova, 1974; G. Maier and Vitiello, 1974; Giulio Maier and Leone Corradi, 1974), that include the inertia effects. This approach has also been included in the more general context of Galerkin methods and finite element applications (L. Corradi, 1990a,b; G. Maier, Comi, et al., 1991). More recently, formulations as optimisation problems of the incremental plasticity problems have been proposed for limit analysis, shakedown analysis, and computational purposes. In (Bisbos et al., 2005; Makrodimopoulos and Martin, 2005a,b), limit and shakedown analyses are done using a second order cone programming technique and quadratic optimisation. In Wieners (2007), the sequential quadratic programming method is used for infinitesimal perfect plasticity. In (K. Krabbenhoft et al., 2007; Kristian Krabbenhoft et al., 2005), very interesting developments are carried out for Mohr-Coulomb yield criterion in the context of cone variational inequality, extending the pioneering works of Berga and Géry De Saxcé (1994) and Hjiaj et al. (2003). In Tangaramvong et al. (2012), the plasticity problem, with perfect and hardening plasticity in quasi-statics, is solved using a complementarity system and mixed finite elements. In Kanno (2016) and Shimizu and Kanno (2020), accelerated gradient algorithms are used to solve the incremental plasticity problem. In Zheng et al. (2020), non-associative plasticity with non-smooth yield surfaces is formulated as a mixed complementarity problem. In Xue Zhang (2014) and subsequent work pieces (Meng et al., 2020; X. Zhang et al., 2013; Xue Zhang, Kristian Krabbenhoft, et al., 2015; Xue Zhang,

Sheng, et al., 2017; Zhao et al., 2022; Zhou et al., 2023), the mathematical programming approach of K. Krabbenhoft et al. (2007) based on a saddle-point problem is further extended to new space-discretization techniques such as PFEM and non-associative flow rule for applications in geotechnics.

Finally, in P. Heng et al. (2016, 2017), Khan, Ahmad, et al. (2021), and Khan, Smith, et al. (2013), the effect of impact in elasto-plastic structures with the help of mathematical programming techniques is studied, but there is no monolithic algorithm to solve the contact and impact multipliers with the plasticity flow rule.

Another fundamental contribution of the nonsmooth mechanics community under the seminal impulse of Moreau is the dynamics of mechanical systems with contact, Coulomb friction and impact. Again, these constitutive laws can be written as variational inequalities and complementarity problems. Unilateral contact in mechanical systems implies jumps in the velocities. For discrete systems, measure differential equations are necessary to formulate rigorously the problem in order to design robust and efficient time–stepping schemes. Without entering into details, our work will be based on the nonsmooth contact dynamics method developed by Jean and J. J. Moreau (1987, 1992) (see also Jean (1999) and J. J. Moreau (1988) for further developments and Vincent Acary and Brogliato (2008) and Dubois et al. (2018) for reviews of the method). In this time-stepping scheme, the velocity and the impulses are the main discrete unknown variables, yielding to a robust and consistent integration scheme. When only unilateral contact and impact are involved, the discrete problem can also be written as an optimisation problem. It seems therefore natural to propose an unified formulation for the problem of elasto-plastic structure subjected to contact conditions and impact, that enables the use of the powerful algorithms developed in the numerical optimisation community.

Contribution and outline of the article The outline of the article is as follows. In Section 2, the equations of the dynamics of an elastoplastic system with unilateral contact are recalled. The goal of this section is, first, to formulate all the equations in a variational framework, respecting the principles of the thermodynamics and second, to write the elastoplastic law and contact law as a variational inequality. These two features allow one to state some energy principles. The formulation starts from the well-known framework of generalised standard materials and is extended to the case of unilateral contact in dynamics. Starting from the continuous time and space formulation, the model is discretized in Section 3. The space discretization is based on a standard iso-parametric finite element application to keep the presentation as simple as possible. We end up with a finite-dimensional differential variational inequality that takes into account the plasticity and the contact constraints at the end of Section 3.1. Since we then deal with finite-dimensional systems with finite masses, the discontinuities in the velocity imply impulsive forces. This is the reason why the system is recast with the help of differential measures and an impact law is introduced in the formulation to close the system equations. In Section 3.2, a time–stepping method is developed on the basis of the Moreau-Jean time stepping scheme. This scheme integrates the nonsmooth dynamics dealing consistently with the impulsive motion. Furthermore, it allows one to give some well-posedness results and a discrete energy balance that ensures that the scheme is well-posed and stable. Some of elements of the literature are relatively closed from our approach, but we differ mainly in the facts that a) we consider explicitly dynamics with impacts in a nonsmooth setting, b) we prove the well-posedness of the one-step problem and c) we give a discrete energy balance that ensures the stability of the scheme. Finally, in Section 4, some numerical illustrations are developed to show the interest of the proposed approach. The method is able to simulate multi-criteria elasto-plastic flow rules with contact constraints. The discrete energy balance highlights which physical processes dissipates the energy. Especially, the question of the coefficient of restitution and the energy dissipated by the impact is discussed with respect to the mesh size and the time-step.

2 Elasto-plasticity dynamics with unilateral contacts

The formulation of a model for the elasto-plasticity dynamics is based on the standard textbooks (Guy T Houlsby and Puzrin, 2007; Maugin, 1992; Nguyen, 2000). The constitutive equations for such elasto-plastic systems involves constraints on the state variables and their derivatives. Typically, the stresses and the forces associated to the hardening parameters are constrained to be in an admissible set defined

by the yield criteria. The most convenient framework for dealing with constraints is Convex Analysis as it has been pioneered by J. J. Moreau (1970, 1986) and Jean Jacques Moreau (1974) in the context of plasticity, friction and contact, introducing super-potentials and pseudo-potentials of dissipation. In this work, the notion of Generalized Standard Materials (GSM) (Halphen and Son Nguyen, 1975) is used for the constitutive models with the Moreau–Ziegler assumption of normal dissipation.

2.1 Principle of virtual powers

The material body is assumed to an open set $\Omega \subset\in \mathbb{R}^d, d \in [\![1,3]\!]$ for $t \in [0,T]$. The volume Lebesgue measure is denoted by $\mathrm{d}v(x)$ and the mass measure is denoted by $\mathrm{d}m(x,t)$. We assume that mass measure has only a density with respect to $\mathrm{d}v(x)$, denoted by $\rho(x,t)$, the density of the material, that is $\mathrm{d}m(x,t) = \rho(x,t)\mathrm{d}v(x)$. Due to the one-sided contact conditions between bodies, the velocity $\boldsymbol{v}(x,t) : \Omega \times [0,T] \to \mathbb{R}^d$ may encounter some jumps in time and space, and is assumed to be a right continuous function of bounded variations i.e. $\boldsymbol{v}(x,t) = \boldsymbol{v}^+(x,t)$. We assume that the set of points (x,t), at which the velocity is discontinuous

$$\mathcal{S} = \{x,t \in \Omega \times [0,T] \mid \boldsymbol{v}^+(x,t) \neq \boldsymbol{v}^-(x,t)\}, \tag{4}$$

is of measure zero with respect to $\mathrm{d}m$. This assumption is standard in solid mechanics of elasto-plastic bodies with shock waves, where it is implicitly assumed that there is no impulsive forces. A discussion on this assumption is made in Remark 1. With these precautions, we can assume that the kinetic energy defined as

$$\mathcal{T}(t) = \frac{1}{2}\int_\Omega \boldsymbol{v}(x,t)\cdot\boldsymbol{v}(x,t)\,\mathrm{d}m(x,t), \tag{5}$$

is a continuous function of time. Its time derivative defines the power of inertial forces as

$$\frac{d}{dt}\mathcal{T}(t) = \mathcal{P}_{\text{inertia}}(t) = \int_\Omega \boldsymbol{v}(x,t)\cdot\dot{\boldsymbol{v}}(x,t)\,\mathrm{d}m(x,t), \tag{6}$$

may be a discontinuous function of time. We can also define the virtual power of inertial forces as

$$\mathcal{P}^\star_{\text{inertia}}(t) = \int_\Omega \boldsymbol{v}^\star(x,t)\cdot\dot{\boldsymbol{v}}(x,t)\,\mathrm{d}m(x,t), \tag{7}$$

where $\boldsymbol{v}^\star$ is the virtual velocity with the same regularity as $v(x,t)$. For the power of internal forces, we assume that the second order symmetric Cauchy stress tensor $\boldsymbol{\sigma} \in T_2^d$ and the tensor of virtual strain rates $\boldsymbol{D}^\star(x,t)$ is discontinuous on a set S_D of zero measure with respect to $\mathrm{d}v(x)$, and that $S \subset S_D$. The tensor of strain rates is in duality with the Cauchy stress tensor $\boldsymbol{\sigma}$ by the power of internal forces as

$$\mathcal{P}^\star_{\text{int}}(t) = -\int_\Omega \boldsymbol{D}^\star(x,t) : \boldsymbol{\sigma}(x,t)\,\mathrm{d}v(x). \tag{8}$$

The virtual power of volume forces $\boldsymbol{f}$, assumed to be a Lebesgue integrable function, is defined by

$$\mathcal{P}^\star_{\text{v}}(t) = \int_\Omega \boldsymbol{v}^\star(x,t)\cdot\boldsymbol{f}(x.t)\,\mathrm{d}v(x). \tag{9}$$

For the power of contact forces, i.e. external forces on the surface boundary $\partial\Omega$, we assume that these forces are splitted into known applied contact external forces, $\boldsymbol{t}(x,t)$, and unknown normal contact forces, denoted $\boldsymbol{r}(x)$ associated with the one-sided contact boundary conditions. The power of applied contact forces is defined as follows

$$\mathcal{P}^\star_{\text{ext}}(t) = \int_{\partial\Omega} \boldsymbol{v}^\star(x,t)\cdot\boldsymbol{t}(x,t)\,\mathrm{d}s(x), \text{ and } \mathcal{P}^\star_{\text{contact}}(t) = \int_{\partial\Omega} \boldsymbol{v}^\star(x,t)\cdot\boldsymbol{r}(x,t)\,\mathrm{d}s(x). \tag{10}$$

Principle of virtual power The principle of virtual power in the setting of classical mechanics postulates that the virtual power of inertial forces balances the virtual power of all other forces, internal, external, volume and contact applied to the system for all virtual velocity fields :

$$\mathcal{P}^{\star}_{\text{inertia}}(t) = \mathcal{P}^{\star}_{\text{v}}(t) + \mathcal{P}^{\star}_{\text{int}}(t) + \mathcal{P}^{\star}_{\text{ext}}(t) + \mathcal{P}^{\star}_{\text{contact}}(t), \quad \forall \boldsymbol{v}^{\star} \tag{11}$$

Energy balance Choosing the virtual field $\boldsymbol{v}^{\star}$ equal to the actual velocity field $\boldsymbol{v}$, we obtain

$$\dot{\mathcal{T}}(t) = \mathcal{P}_{\text{v}}(t) + \mathcal{P}_{\text{int}}(t) + \mathcal{P}_{\text{ext}}(t) + \mathcal{P}_{\text{contact}}(t). \tag{12}$$

Remark 1. *The assumptions we made in this section are usually found in the mechanical literature on continuum mechanics with discontinuities, especially, with shocks waves in elasto-plastic solids, for instance in (Davison, 2008; Germain and E. Lee, 1973; E. H. Lee and Liu, 1964; Mandel, 1964). From a mathematical point of view, they are generally not sufficient to define correctly the problem in a more general framework and the question of existence and uniqueness. This needs further mathematical setting, that are far beyond the scope of the paper. Especially, the regularity and the bodies in which we can write the equations of conservation. In this article, we assume smooth surfaces of discontinuities but more generally, geometric measure theory must be called to define subbodies, normal to surfaces and Cauchy stress (see for instance (Gurtin et al., 1987; Musesti, 2001)).*

The assumption about the set of discontinuities if of zero measure with respect to $\mathrm{d}m$ *is also questionable, even though the mass has only a density with respect to the volume or surface measure. When some one-sided constraints are imposed on elastic bodies in dynamics, the question of the existence and the regularity of solutions remains an open question. In a seminal paper, Lebeau and Schatzman (1984) show the existence and uniqueness of solutions and prove the conservation of energy for an elastic half-space with Signorini condition, where there is no impulsive forces, or impulsive stresses. In dimension* 1*, it corresponds to the equation of elastic bar and in dimension* 2*, to a membrane. For a more general object, in particular, a manifold of co-dimension* 1 *in* $\mathbb{R}^d$ *(beams, plates, shells), the question is open and simple examples show that impulsive forces are possible.*

2.2 Elasto-plasticity in the Generalized Standard Material (GSM) setting

For the formulation of the elasto-plastic behavior of the continuous medium, we assume that we are in the framework the small-perturbation hypothesis (SPH). We also assume that these equations are written where the tensor of strain rates $\boldsymbol{D}$ is well defined.

$$\boldsymbol{D}(x,t) = \dot{\boldsymbol{\varepsilon}}(x,t), \tag{13}$$

where the second order symmetric strain tensor $\boldsymbol{\varepsilon}$ is given by $\boldsymbol{\varepsilon}(\boldsymbol{u}) = \nabla_s(\boldsymbol{u}) = \frac{1}{2}(\nabla^{\top}(\boldsymbol{u}) + \nabla(\boldsymbol{u}))$ (∇ denotes the gradient). As usual under the SPH, the strain tensor is decomposed in an additive way into an elastic part, *i.e.* the reversible part of the strain, and a plastic part as follows

$$\boldsymbol{\varepsilon} = \boldsymbol{\varepsilon}^e + \boldsymbol{\varepsilon}^p. \tag{14}$$

The presentation of the elasto-plastic model with hardening is made in the framework of generalized standard materials (Halphen and Son Nguyen, 1975; Maugin, 1992) in order to satisfy the principles of thermo-mechanics.

Free energy and state laws We start by the definition of the free energy per unit of volume $\psi(\boldsymbol{\varepsilon}^e, \boldsymbol{\alpha})$ in the isothermal setting (the free energy does not depend on the temperature T) assuming a separation in $\boldsymbol{\varepsilon}^e$ and $\boldsymbol{\alpha}$:

$$\psi(\boldsymbol{\varepsilon}^e, \boldsymbol{\alpha}) = \psi^e(\boldsymbol{\varepsilon}^e) + \psi^p(\boldsymbol{\alpha}), \tag{15}$$

where $\boldsymbol{\alpha}$ is an order-one tensor of hardening parameters, ψ^e is the elastic potential energy and ψ^p is the plastic potential energy due to the hardening process. The state laws govern the generalized (driving)

forces $\boldsymbol{\sigma}(x,t) \in T^d$ and $\boldsymbol{a}(x,t)$ as the derivative of the free energy:

$$\boldsymbol{\sigma} = \frac{\partial \psi(\boldsymbol{\varepsilon}^e, \boldsymbol{\alpha})}{\partial \boldsymbol{\varepsilon}^e}, \quad \text{and} \quad \boldsymbol{a} = \frac{\partial \psi(\boldsymbol{\varepsilon}^e, \boldsymbol{\alpha})}{\partial \boldsymbol{\alpha}}. \tag{16}$$

In the simplest case, quadratic potentials are chosen,

$$\psi^e(\boldsymbol{\varepsilon}^e) = \frac{1}{2}\boldsymbol{\varepsilon}^e : \mathbf{E} : \boldsymbol{\varepsilon}^e \quad \text{and} \quad \psi^p(\boldsymbol{\alpha}) = \frac{1}{2}\boldsymbol{\alpha} \cdot \mathbf{D} \cdot \boldsymbol{\alpha} \tag{17}$$

with $\mathbf{E}$ a symmetric 4-th order elastic tensor and $\mathbf{D}$ a symmetric second order tensor, the state laws are then linear :

$$\boldsymbol{\sigma} = \mathbf{E} : \boldsymbol{\varepsilon}^e \quad \text{and } \boldsymbol{a} = \mathbf{D} \cdot \boldsymbol{\alpha}. \tag{18}$$

Intrinsic dissipation From the first and second principles of thermodynamics, the intrinsic dissipation per unit of volume d in a isothermal setting, defined by

$$d = \boldsymbol{\sigma} : \dot{\boldsymbol{\varepsilon}} - \dot{\psi}(\boldsymbol{\varepsilon}^e, \boldsymbol{\alpha}), \tag{19}$$

must be positive. Developing $\dot{\psi}(\boldsymbol{\varepsilon}^e, \boldsymbol{\alpha})$, we get

$$d = \boldsymbol{\sigma} : \dot{\boldsymbol{\varepsilon}} - \left[\frac{\partial \psi(\boldsymbol{\varepsilon}^e, \boldsymbol{\alpha})}{\partial \boldsymbol{\varepsilon}^e} : \dot{\boldsymbol{\varepsilon}}^e + \frac{\partial \psi(\boldsymbol{\varepsilon}^e, \boldsymbol{\alpha})}{\partial \boldsymbol{\alpha}} \cdot \dot{\boldsymbol{\alpha}} \right]. \tag{20}$$

With the state laws defined above, this can be simplified in

$$d = \boldsymbol{\sigma} : \dot{\boldsymbol{\varepsilon}} - [\boldsymbol{\sigma} : \dot{\boldsymbol{\varepsilon}}^e + \boldsymbol{a} \cdot \dot{\boldsymbol{\alpha}}] = \boldsymbol{\sigma} : [\dot{\boldsymbol{\varepsilon}} - \dot{\boldsymbol{\varepsilon}}^e] - \boldsymbol{a} \cdot \dot{\boldsymbol{\alpha}} = \boldsymbol{\sigma} : \dot{\boldsymbol{\varepsilon}}^p - \boldsymbol{a} \cdot \dot{\boldsymbol{\alpha}}. \tag{21}$$

The total intrinsic dissipation (or dissipated power) $\mathcal{D}(t)$ and the total free energy Ψ is defined as

$$\mathcal{D}(t) = \int_\Omega d(x,t)\,\mathrm{d}x, \text{ and } \Psi(t) = \int_\Omega \psi(\boldsymbol{\epsilon}^e(x,t), \boldsymbol{\alpha}(x,t))\,\mathrm{d}x. \tag{22}$$

Then, the power of internal forces is expressed as

$$\mathcal{P}_{\text{int}}(t) = -\int_\Omega d(x,t)\,\mathrm{d}x - \int_\Omega \dot{\psi}(\boldsymbol{\epsilon}^e(x,t), \boldsymbol{\alpha}(x,t))\,\mathrm{d}x, \tag{23}$$

that is

$$\mathcal{P}_{\text{int}}(t) = -\mathcal{D}(t) - \dot{\Psi}(t). \tag{24}$$

For a detailed energy balance in the context of elastoplasticity with hardening, we refer to (Chrysochoos et al., 1989).

Normality rule and complementary laws From the second principle of the thermodynamics, the intrinsic dissipation must satisfy the Clausius-Duhem inequality, that is, in an isothermal setting

$$d = \boldsymbol{\sigma} : \dot{\boldsymbol{\varepsilon}}^p - \boldsymbol{a} \cdot \dot{\boldsymbol{\alpha}} \geqslant 0. \tag{25}$$

A convenient way to ensure that complementary laws will imply this inequality is to postulate the existence of a pseudo potential of dissipation from which the rate of changes of the $\boldsymbol{\varepsilon}^p$ and $\boldsymbol{\alpha}$ derive (Jean Jacques Moreau, 1974). In the case of elasto-plastic models that obey to the normality rule (associated plasticity), we introduce a convex set $\boldsymbol{C}$ as the set of admissible stresses $\boldsymbol{\sigma}$ and forces $\boldsymbol{a}$, and the complementary laws are defined by the following differential inclusion

$$\begin{pmatrix} \dot{\boldsymbol{\varepsilon}}^p \\ -\dot{\boldsymbol{\alpha}} \end{pmatrix} \in N_{\boldsymbol{C}} \begin{pmatrix} \boldsymbol{\sigma} \\ \boldsymbol{a} \end{pmatrix}. \tag{26}$$

The complementary laws (26) imply the Clausius-Duhem inequality (25) if the origin belongs to $\boldsymbol{C}$. Using the definition of the normal cone (2), the complementary laws are equivalent to the following variational inequality

$$\dot{\boldsymbol{\varepsilon}}^p : (\boldsymbol{\sigma} - \hat{\boldsymbol{\sigma}}) - \dot{\boldsymbol{\alpha}} \cdot (\boldsymbol{a} - \hat{\boldsymbol{a}}) \geqslant 0, \quad \forall (\hat{\boldsymbol{\sigma}}, \hat{\boldsymbol{a}}) \in \boldsymbol{C}, \tag{27}$$

also know as the Hill's principle of maximum dissipation

$$\dot{\boldsymbol{\varepsilon}}^p : \boldsymbol{\sigma} - \dot{\boldsymbol{\alpha}} \cdot \boldsymbol{a} \geqslant \dot{\boldsymbol{\varepsilon}}^p : \hat{\boldsymbol{\sigma}} - \dot{\boldsymbol{\alpha}} \cdot \hat{\boldsymbol{a}}, \quad \forall (\hat{\boldsymbol{\sigma}}, \hat{\boldsymbol{a}}) \in \boldsymbol{C}. \tag{28}$$

2.3 Unilateral contact

In this work, the unilateral contact is considered as perfect unilateral constraint. Let us assume that we are able to define the normal gap function $g_{\text{N}}(x)$ between two points of the boundary of Ω that are candidate to contact. To simplify the presentation, we assume that there is no explicit dependence of the gap function on time. The normal relative velocity v_{N} is defined as the time derivative of the gap function

$$v_{\text{N}}(x,t) = \dot{g}_{\text{N}}(x) = \nabla_x g(x) \cdot \boldsymbol{v}(x,t) := \boldsymbol{H}(x) \cdot \boldsymbol{v}(x,t). \tag{29}$$

The normal reaction at contact r_{N} is defined by duality using the virtual power of contact forces as

$$\mathcal{P}^{\star}_{\text{contact}}(t) \quad = \quad \int_{\partial\Omega} \boldsymbol{v}^{\star}(x,t) \cdot \boldsymbol{r}(x,t)\, \mathrm{d}s(x) = \int_{\partial\Omega} v^{\star}_{\text{N}}(x,t) r_{\text{N}}(x,t)\, \mathrm{d}s(x), \tag{30}$$

and hence, using (29),

$$\boldsymbol{r}(x,t) = \boldsymbol{H}(x) r_{\text{N}}(x,t). \tag{31}$$

The Signorini condition can be viewed as an additional state law associated with the additional state variable g_{N}. The surface free energy ψ^s of the system is defined with the indicator function of $\mathbb{R}_+$, $\mathrm{i}_{\mathbb{R}_+}$, taken at g_{N}

$$\psi^s(g_{\text{N}}) = \mathrm{i}_{\mathbb{R}_+}(g_{\text{N}}). \tag{32}$$

The Signorini condition is then obtained by sub-differentiating

$$-r_{\text{N}} \in \partial_{g_{\text{N}}} \psi^s(g_{\text{N}}) = \partial \mathrm{i}_{\mathbb{R}_+}(g_{\text{N}}) \iff -r_{\text{N}} \in \mathrm{N}_{\mathbb{R}_+}(g_{\text{N}}). \tag{33}$$

The definition of the subdifferential of the indicator function leads to the signorini condition in terms of complementarity:

$$0 \leqslant g_{\text{N}} \perp r_{\text{N}} \geqslant 0. \tag{34}$$

It is also possible to write a stronger condition at the velocity level that implies the standard Signorini condition as

$$-r_{\text{N}} \in N_{T_{\mathbb{R}_+}(g_{\text{N}})}(v_{\text{N}}), \tag{35}$$

where $T_{\mathbb{R}_+}(g_{\text{N}})$ is the tangent cone of $\mathbb{R}_+$ (see J. J. Moreau (1988)). Equivalently, the complementarity condition at the velocity level is

$$0 \leq r_{\text{N}} \perp v_{\text{N}} \geq 0 \text{ if } g_{\text{N}} = 0, \text{ else } r_{\text{N}} = 0. \tag{36}$$

Power of contact forces. The power done by the contact forces vanishes almost everywhere due to (36), does not dissipate or release energy:

$$\mathcal{P}_{\text{contact}}(t) = \int_{\partial\Omega} \boldsymbol{r}(x,t) \cdot \boldsymbol{v}(x,t)\, \mathrm{d}s(x) = \int_{\partial\Omega} r_{\text{N}}(x,t) v_{\text{N}}(x,t)\, \mathrm{d}s(x) = 0. \tag{37}$$

3 Space and Time discretizations

3.1 Standard finite element discretization

In this section, we introduce a standard finite element discretization of the elasto-plastic bodies. We have chosen to leave it as simple as possible since this is not the main objective of the paper. For a comprehensive review of the specifity of finite element application to plasticity, we refer to Nodargi (2019) where enhanced mixed FE discretization can be found. The FE discretization of the displacement in an element labeled by $e \in [\![1, n_{\text{el}}]\!]$ is given by

$$u_e(x) = \bar{N}_e(x) u_e = N_e(x) u, \tag{38}$$

where $u_e \in \mathbb{R}^{d_u}$ is the vector composed of the nodal displacements of the element and $u \in \mathbb{R}^n$ the nodal displacement vector of the whole structure. The matrix N_e denotes the shape function matrix of the element e.

Note that u is not the simple concatenation of u_e, in other words $u \neq \text{col}(u_e, e \in [\![1, n_{\text{el}}]\!])$ but is related by a local-to-global mapping A_e such that $u_e = A_e u$. This mapping is also used for the assembly of the structural matrices. To avoid too complex notation related to the assembly process, we prefer to formulate the problem directly with $N_e(x)$ (see Bathe, 1996).

The strain, in vector notation, $\varepsilon_e \in \mathbb{R}^{d_\varepsilon}$, using Voigt notation in an element is given by

$$\varepsilon_e(x) = B_e(x) u, \tag{39}$$

where $B_e(x)$ is the strain-displacement matrix for the element e obtained by applying (38) in the definition of the strain tensor from the displacement. The nodal velocity vector v_e is assumed to be given by the time derivative of the nodal displacement vector leading to

$$v_e(x) = N_e(x) v. \tag{40}$$

Using the same Galerkin approximation for virtual velocities, the principle of virtual power yields the following space discretized equation for the element e

$$\begin{aligned} \int_{\Omega_e} N_e^\top(x) N_e(x) \mathrm{d}m(x,t)\ \dot{v}(t) + \int_{\Omega_e} B_e^\top(x) \sigma(x,t) \mathrm{d}v(x) = \\ \int_{\Omega_e} N_e^\top(x) f(x,t) \mathrm{d}v(x) + \int_{\partial\Omega_e} N_e^\top(x) \tau(x,t) \mathrm{d}s(x) + \int_{\partial\Omega_e} N_e^\top(x) r(x,t) \mathrm{d}s(x). \end{aligned} \tag{41}$$

Using the following standard notation,

$$M_e(t) = \int_{\Omega_e} N_e^\top(x) N_e(x) \mathrm{d}m(x,t), \tag{42}$$

for the consistent mass matrix, and

$$\begin{aligned} f_{\text{int},e}(t) &= \int_{\Omega_e} B_e^\top(x) \sigma(x,t) \mathrm{d}v(x) \\ f_{\text{ext},e}(t) &= \int_{\Omega_e} N_e^\top(x) f(x,t) \mathrm{d}v(x) + \int_{\partial\Omega_e} N_e^\top(x) \tau(x,t) \mathrm{d}s(x) \\ r_{\text{contact},e}(t) &= \int_{\partial\Omega_e} N_e^\top(x) r(x,t) \mathrm{d}s(x), \end{aligned} \tag{43}$$

for the nodal internal, external and contact forces, we obtain the contribution to equation of motion of the element e as

$$M_e(t)\dot{v}(t) + f_{\text{int},e}(t) = f_{\text{ext},e}(t) + r_{\text{contact},e}(t). \tag{44}$$

For the whole bodies Ω, the equation are obtained by summing the contributions of the elements yielding

$$M(t)\dot{v}(t) + f_{\text{int}}(t) = f_{\text{ext}}(t) + r_{\text{contact}}(t). \tag{45}$$

with

$$M(t) = \sum_{e=1}^{n_{\text{el}}} M_e(t), f_{\text{int}}(t) = \sum_{e=1}^{n_{\text{el}}} f_{\text{int},e},\ f_{\text{ext}}(t) = \sum_{e=1}^{n_{\text{el}}} f_{\text{ext},e},\ \text{and } r_{\text{contact}}(t) = \sum_{e=1}^{n_{\text{el}}} r_{\text{contact},e}. \quad (46)$$

Equilibrium matrix In order to obtain a convenient matrix notation for the internal forces, we note that the internal forces are linear in σ_e. A discretization of the stresses $\sigma_e(x,t)$ in the element should result in a linear formulae expressed as a matrix product with the introduction of an equilibrium matrix. In the sequel, we use the discretization directly based in the Gauss quadrature rule for evaluating the integrals. More enhanced approaches as been discussed in (Leone Corradi, 1985). Using the discrete equilibrium matrix B defined in Appendix A, we get the matrix from of the internal forces as

$$f_{\text{int},e} = B_e^T \sigma_e, \text{ and } f_{\text{int}} = \sum_{e=1}^{n_{\text{el}}} f_{\text{int},e} = B^T \sigma. \quad (47)$$

Hence, the space-discretized equation of motion (45) reads as

$$M(t)\dot{v}(t) + B^T \sigma(t) = f_{\text{ext}}(t) + r_{\text{contact}}(t). \quad (48)$$

Remark 2. *In Appendix A, the strain and stress discrete values are gathered into column vector using a scaling by the square root of the Gauss weights. This allows a convenient matrix notation, where the structure equilibrium matrix is directly the adjoint operator of the strain-displacement matrix as in standard force method (see for instance (Pellegrino, 1993)). It would also have been possible to introduce another diagonal matrix containing the Gauss weight leading to a direct gathering without scaling of the strain and stress values at Gauss points.*

Discretization of the elasto-plastic equations Since the stress and strain vectors are evaluated at Gauss points, we choose to apply directly the elastoplastic model at the gauss points. It results in the following system of equation in matrix vector notation:

$$\begin{cases} \sigma = E\varepsilon^e = E(\varepsilon - \varepsilon^p) \\ a = D\alpha \\ \begin{pmatrix} \dot{\varepsilon}^p \\ -\dot{\alpha} \end{pmatrix} \in N_C \begin{pmatrix} \sigma \\ a \end{pmatrix}, \end{cases} \quad (49)$$

where E is the elasticity matrix obtained by reformulating the elasticity tensor $\boldsymbol{E}$ in matrix with Voigt notation for instance. The same applies for $\boldsymbol{D}$. The only point of attention is the definition of the convex set C that is a Cartesian product of the set $\boldsymbol{C}$ for each Gauss points and taking into account the scaling due to the Gauss weights introduced in appendix A.

Discretization of the contact conditions The discretization of the contact conditions is a delicate subject. An accurate discretization of the contact traction $\boldsymbol{r}(x,t)$ call for the use of mortar finite element techniques (see for instance (Belgacem et al., 1998; Popp et al., 2009)). Since it is beyond the scope of the article and to keep the presentation as simple as possible, the discretization is made by choosing to apply the Signorini condition to a set of discrete points on the contact boundary associated with point load contact forces. These discrete points can be simply a node of the mesh, or a point for which the position is expressed in terms of the node displacements in a iso-parametric setting, with the shape function matrix. For a contact point labeled by $\alpha \in [\![1 \dots m]\!]$, the gap function is written as a function of the nodal displacement u as $g_{\text{N}}^\alpha(u)$. The normal relative velocity is then given by

$$v_{\text{N}}^\alpha = \frac{d}{dt} g_{\text{N}}(u) = \nabla_u^\top (g_{\text{N}}^\alpha(u)) v := H^{\alpha,\top}(u) v. \quad (50)$$

The vector v_{N} is defined by collecting all the relative velocities at the contacts points, $v_{\text{N}} := \text{col}(v_{\text{N}}^\alpha, \alpha \in [\![1, m]\!])$, and the matrix H is defined as

$$v_{\text{N}} = H^\top(u) v. \quad (51)$$

By duality, the contact forces are expressed as

$$r^\alpha = H^\alpha(u) r_{\text{N}}^\alpha, \text{ and } r_{\text{contact}} = H(u) r_{\text{N}}^\alpha. \tag{52}$$

The Signorini condition at the velocity level is then written as

$$-r_{\text{N}} \in N_{T_{\mathbb{R}^m_+}(g_{\text{N}}(t))}(v_{\text{N}}). \tag{53}$$

Nonsmooth dynamics for finite-freedom mechanical systems Once the space-discretization is performed, we end up with a finite freedom mechanical system that is subjected to unilateral constraints. In standard finite element discretization, all degrees of freedom possess a finite mass. Since the system may encounter some jumps in the velocities, the fact that we have mass finite masses leads to the possibility to have percussion in the dynamics. In other words, the assumption that we made in Section 2.1 is no longer valid and we need to take into account the velocity jump into the equation of motion. To this aim, we consider that the velocity is a right continuous function of bounded variations with respect to time and the acceleration is therefore considered as a differential measure $\mathrm{d}v$ associated with v (J. Moreau, 1988). We will further assume that the reaction due to the unilateral constraint is also a measure denoted by $\mathrm{d}i_{\text{N}}$ that have the same support as $\mathrm{d}v$. Assuming that the internal forces have only a density with the Lebesgue measure, the equation of motion

$$M(t)\dot{v}(t) + B^T\sigma(t) = f_{\text{ext}}(t) + H(u(t))r_{\text{N}}(t), \tag{54}$$

is extended as measure equation as

$$M\mathrm{d}v + B^\top\sigma(t)\mathrm{d}t = f_{\text{ext}}(t)\mathrm{d}t + H(u(t))\mathrm{d}i_{\text{N}}. \tag{55}$$

If we define r_{N} as the density of $\mathrm{d}i_{\text{N}}$ with respect to the Lebesgue measure, the equation (54) appears as the equation of motion, valid almost everywhere. At any time point t_i, the measure equation amounts to solving the impact equation

$$M(v(t_i) - v^-(t_i)) = H(u(t_i))p_{i,\text{N}}, \tag{56}$$

where the percussion $p_{i,\text{N}}$ is the normal percussion, *i.e.* the density of $\mathrm{d}i_{\text{N}}$ with respect to the Dirac atom at t_i. In order to solve the system with a new unknown $p_{i,\text{N}}$, we need to introduce an impact law. The simplest choice if the Newton impact law

$$v_{\text{N}}^\alpha(t_i) = -ev_{\text{N}}^{\alpha,-}(t_i), \quad \text{if } g_{\text{N}}^\alpha(u(t_i)) = 0 \text{ and } v_{\text{N}}^{\alpha,-}(t_i) \leq 0, \tag{57}$$

where e is the Newton coefficient of restitution. Following the seminal work of J. J. Moreau (1988), the Newton impact law and the contact law expressed in (53) are formulated as a measure inclusion as

$$-\mathrm{d}i_{\text{N}} \in N_{T_{\mathbb{R}^m_+}(g_{\text{N}}(t))}(v_{\text{N}}(t) + ev_{\text{N}}^-(t)). \tag{58}$$

Summary of the space-discretized equations To sum-up, after the space discretization, the equations of the elasto-plastic system with unilateral contact read as

$$\begin{cases} M\mathrm{d}v + B^\top\sigma(t)\mathrm{d}t = f_{\text{ext}}(t)\mathrm{d}t + H(u(t))\mathrm{d}i_{\text{N}} \\ \dot{u}(t) = v(t) \\ \sigma(t) = E(\varepsilon(t) - \varepsilon^p(t)) \\ a(t) = D\alpha(t) \\ \begin{pmatrix} \dot{\varepsilon}^p(t) \\ -\dot{\alpha}(t) \end{pmatrix} \in N_C \begin{pmatrix} \sigma(t) \\ a(t) \end{pmatrix} \\ v_{\text{N}}(t) = H^\top(u(t))v(t) \\ -\mathrm{d}i_{\text{N}} \in N_{T_{\mathbb{R}^m_+}(g_{\text{N}}(t))}(v_{\text{N}}(t) + ev_{\text{N}}^-(t)). \end{cases} \tag{59}$$

In order to prepare the time discretization of (59), the differential equation are separated from the algebraic equations and the normal cone inclusion introducing two slack variables $y = \dot{\alpha}$ and $z = -\dot{\varepsilon}^p$.

Assuming that the elastic law is valid at time t_0, that is, $\sigma(t_0) = E\varepsilon(t_0)$, the elasticity can be expressed as

$$\dot{\sigma}(t) = E(\dot{\varepsilon}(t) - \dot{\varepsilon}^p(t)) = E(Bv(t) + z(t)), \tag{60}$$

or equivalently, with the compliance matrix $S = E^{-1}$ as

$$S\dot{\sigma}(t) = Bv(t) + z(t). \tag{61}$$

With the slack variable y and assuming that $a(t_0) = D\alpha(t_0)$, the linear hardening law reads

$$D^{-1}\dot{a}(t) = \dot{\alpha}(t) = y(t). \tag{62}$$

Finally, with the slack variables y and z, the normal cone inclusion for the plasticity flow rule is given by

$$-\begin{pmatrix} z \\ y \end{pmatrix} \in N_C \begin{pmatrix} \sigma \\ a \end{pmatrix}. \tag{63}$$

The complete system of equations for the elasto-plastic evolution with contact reduces to

$$\begin{cases} M\mathrm{d}v + B^\top \sigma(t)\mathrm{d}t = f_{\text{ext}}(t)\mathrm{d}t + H(u(t))\mathrm{d}i_{\text{N}} \\ \dot{u}(t) = v(t) \\ S\dot{\sigma}(t) = Bv(t) + z(t) \\ D^{-1}\dot{a}(t) = y(t) \\ -\begin{pmatrix} z(t) \\ y(t) \end{pmatrix} \in N_C \begin{pmatrix} \sigma(t) \\ a(t) \end{pmatrix} \\ v_{\text{N}}(t) = H^\top(u(t))v(t) \\ -\mathrm{d}i_{\text{N}} \in N_{T_{\mathbb{R}^m_+}(g_{\text{N}}(t))}(v_{\text{N}}(t) + ev_{\text{N}}^-(t)). \end{cases} \tag{64}$$

3.2 Time discretization with an extended Moreau–Jean time–stepping schemes

The time-discretization of the system (64) is given by an extension of the Moreau–Jean scheme for nonsmooth dynamics (Jean and J. J. Moreau, 1987) and by the catching-up algorithm for plasticity (J. J. Moreau, 1976). The dynamics equation in the first line of (64) is discretized using the definition of the differential measure over a time interval $(t_k, t_{k+1}]$ as

$$\int_{(t_k,t_{k+1}]} M\mathrm{d}v = M(v^+(t_{k+1}) - v^+(t_k)) = -\int_{t_k}^{t_{k+1}} B^\top \sigma(t)\mathrm{d}t + \int_{t_k}^{t_{k+1}} f_{\text{ext}}(t)\mathrm{d}t + \int_{(t_k,t_{k+1}]} H(u(t))\mathrm{d}i_{\text{N}}. \tag{65}$$

As in the original Moreau–Jean scheme, the impulse of the reaction measure is kept as primary variable to ensure consistency of the scheme when an impact occurs:

$$\int_{(t_k,t_{k+1}]} H(u(t))\mathrm{d}i_{\text{N}} \approx H(u_k)p_{\text{N},k+1}. \tag{66}$$

The explicit approximation of $H(u(t))$ is justified by the fact that we assume to be under the small perturbations hypothesis. Using the following standard notation x_k and x_{k+1} for the approximations of the function $x(t)$ at time t_k and t_{k+1}, the remaining nonimpulsive terms of (39) are approximated with a $\theta-$method as

$$M(v_{k+1} - v_k) + hB^\top \sigma_{k+\theta} = hf_{\text{ext,k}+\theta} + H(u_k)p_{\text{N},k+1}, \tag{67}$$

where the following notation is used $x_{k+\theta} = \theta x_{k+1} + (1-\theta)x_k$ for any variable x. The non impulsive dynamical equations in (64) are also discretized using a $\theta-$method

$$\begin{aligned} &u_{k+1} = u_k + hv_{k+\theta}, \\ &S(\sigma_{k+1} - \sigma_k) - hBv_{k+\theta} = hz_{k+\theta}, \\ &D^{-1}(a_{k+1} - a_k) = hy_{k+\theta}. \end{aligned} \tag{68}$$

The normal cone inclusion governing the plastic flow rule is discretized as follows for $\theta > 0$

$$-\begin{pmatrix} z_{k+\theta} \\ y_{k+\theta} \end{pmatrix} \in N_C \begin{pmatrix} \sigma_{k+\theta} \\ a_{k+\theta} \end{pmatrix}. \tag{69}$$

For the contact impact condition, the active constraints at the velocity level must be selected. To this aim, the following index set of contact is introduced

$$\mathcal{I}_k = \{\alpha \mid g_{\mathrm{N},k}^{\alpha} \leq 0, v_{\mathrm{N},k}^{\alpha} \leq 0\} \tag{70}$$

with $v_{\mathrm{N},k}^{\alpha} = H^{\alpha,\top} v_k$. Hence, the impact law is written as

$$\begin{cases} -p_{\mathrm{N},k+1}^{\alpha} \in \mathrm{N}_{\mathbb{R}^+}(v_{\mathrm{N},k+1}^{\alpha} + v_{\mathrm{N},k}^{\alpha}), & \text{for } \alpha \in \mathcal{I}_k \\ p_{\mathrm{N},k+1}^{\alpha} = 0, & \text{otherwise.} \end{cases} \tag{71}$$

where $v_{\mathrm{N},k+1}^{\alpha} = H^{\alpha,\top} v_{k+1}$. By collecting only the contact variables for the index set $\mathcal{I}_k$ as $v_{\mathrm{N}} := \mathrm{col}(v_{\mathrm{N}}^{\alpha}, \alpha \in \mathcal{I}_k)$ and $p_{\mathrm{N}} := \mathrm{col}(p_{\mathrm{N}}^{\alpha}, \alpha \in \mathcal{I}_k)$, the contact impact law is given by

$$-p_{\mathrm{N},k+1} \in \mathrm{N}_{\mathbb{R}_+^m}(v_{\mathrm{N},k+1} + e\, v_{\mathrm{N},k}), \tag{72}$$

where m is the cardinal of $\mathcal{I}_k$. Using the reduced matrix $H = \mathrm{col}(H^{\alpha}, \alpha \in \mathcal{I}_k)$, we also have $v_{\mathrm{N},k} = H^{\top} v_k$ and

$$M(v_{k+1} - v_k) + hB^{\top}\sigma_{k+\theta} = hf_{\mathrm{ext,k}+\theta} + Hp_{\mathrm{N},k+1}. \tag{73}$$

Summary of the space and time discretized equations Altogether, the space and time discretized equations are given by

$$\begin{cases} M(v_{k+1} - v_k) + hB^{\top}\sigma_{k+\theta} = hf_{\mathrm{ext,k}+\theta} + Hp_{\mathrm{N},k+1} \\ S(\sigma_{k+1} - \sigma_k) - hBv_{k+\theta} = hz_{k+\theta}, \\ D^{-1}(a_{k+1} - a_k) = hy_{k+\theta} \\ v_{\mathrm{N},k+1} = H^{\top} v_{k+1} \\ -\begin{pmatrix} z_{k+\theta} \\ y_{k+\theta} \\ p_{\mathrm{N},k+1} \end{pmatrix} \in N_{C\times\mathbb{R}_+^m} \begin{pmatrix} \sigma_{k+\theta} \\ a_{k+\theta} \\ v_{\mathrm{N},k+1} + ev_{\mathrm{N},k} \end{pmatrix} \end{cases} \tag{74}$$

where $u_{k+1} = u_k + hv_{k+\theta}$ can be solved afterwards. Using the relation $x_{k+\theta} - x_k = \theta(x_{k+1} - x_k)$, the discretized equations can be formulated in terms of variables approximated at $t_{k+\theta}$

$$\begin{cases} M(v_{k+\theta} - v_k) + h\theta B^{\top}\sigma_{k+\theta} = h\theta f_{\mathrm{ext,k}+\theta} + \theta Hp_{\mathrm{N},k+1} \\ S(\sigma_{k+\theta} - \sigma_k) - h\theta Bv_{k+\theta} = h\theta z_{k+\theta}, \\ D^{-1}(a_{k+\theta} - a_k) = h\theta y_{k+\theta} \\ \theta v_{\mathrm{N},k+1} = H^{\top} v_{k+\theta} - (1-\theta)v_{\mathrm{N},k} \\ -\begin{pmatrix} z_{k+\theta} \\ y_{k+\theta} \\ v_{\mathrm{N},k+1} + ev_{\mathrm{N},k} \end{pmatrix} \in N_{C\times\mathbb{R}_+^m} \begin{pmatrix} \sigma_{k+\theta} \\ a_{k+\theta} \\ p_{\mathrm{N},k+1} \end{pmatrix} \end{cases}. \tag{75}$$

3.3 Well-posedness

To study the well posedness to the problem (75), we propose to show that it corresponds to the optimality conditions of a saddle point problem, and then to show that this saddle point problem admits a unique solution.

A saddle point problem. Let us consider the following saddle point problem

$$\begin{array}{ll} \min_{v,\dot{\varepsilon}} \max_{\sigma,a} & \frac{1}{2}(v-v_k)^\top M(v-v_k) - \frac{1}{2}(\sigma-\sigma_k)^\top S(\sigma-\sigma_k) - \frac{1}{2}(a-a_k)^\top D^{-1}(a-a_k) \\ & \quad +h\theta\sigma^\top\dot{\varepsilon} - h\theta f_{\text{ext,k+1}}^\top v \\ \text{s.t.} & Bv = \dot{\varepsilon} \\ & \theta v_{\text{N}} = H^\top v - (1-\theta)v_{\text{N},k} \\ & \begin{pmatrix} \sigma \\ a \\ v_{\text{N}} + ev_{\text{N},k} \end{pmatrix} \in C \times \mathbb{R}^m_+. \end{array} \tag{76}$$

Let us introduce the following assumptions

Assumption 1. *The matrices M, S and D are symmetric definite positive matrices.*

Assumption 2. *It exists v^0, σ^0, a^0 such that*

$$\begin{cases} \begin{pmatrix} \sigma^0 \\ a^0 \end{pmatrix} \in C \\ H^\top v^0 + (\theta(1+e)-1)v_{\text{N},k} \geq 0 \end{cases} \tag{77}$$

Proposition 1. *Under Assumptions 1 and 2, the problem (76) has a unique solution $(v, \dot{\varepsilon}, \sigma, a, v_{\text{N}})$.*

To prove that the minimax problem has solutions, *i.e.* saddle points exist, we consider a reduced version of the problem (76) where the equality constraints $Bv = \dot{\varepsilon}$ and $\theta v_{\text{N}} = H^\top v - (1-\theta)v_{\text{N},k}$ are substituted. This yields a reduced saddle point point

$$\begin{array}{ll} \min_{v} \max_{\sigma,a} & \frac{1}{2}(v-v_k)^\top M(v-v_k) - \frac{1}{2}(\sigma-\sigma_k)^\top S(\sigma-\sigma_k) - \frac{1}{2}(a-a_k)^\top D^{-1}(a-a_k) \\ & \quad +h\theta\sigma^\top Bv - h\theta f_{\text{ext,k+1}}^\top v \\ \text{s.t.} & \begin{pmatrix} \sigma \\ a \\ H^\top v + (\theta(1+e)-1)v_{\text{N},k} \end{pmatrix} \in C \times \mathbb{R}^m_+. \end{array} \tag{78}$$

with its associated Lagrangian function of the form

$$\begin{aligned} \bar{\mathcal{L}}(v,\sigma,a) \quad = \quad & \frac{1}{2}(v-v_k)^\top M(v-v_k) - \frac{1}{2}(\sigma-\sigma_k)^\top S(\sigma-\sigma_k) - \frac{1}{2}(a-a_k)^\top D^{-1}(a-a_k) \\ & +h\theta\sigma^\top Bv - h\theta f_{\text{ext,k+1}}^\top v - h\theta\Psi_C\begin{pmatrix}\sigma\\ a\end{pmatrix} + \theta^2\Psi_{\mathbb{R}^m_+}(H^\top v + (\theta(1+e)-1)v_{\text{N},k}). \end{aligned} \tag{79}$$

Assuming that M, S and D are symmetric definite positive matrices, the Lagrangian function $\bar{\mathcal{L}}$ is a convex function in v and a concave function of (σ, a). With the assumption (77) , the following coercivity properties hold:

$$\lim_{\|v\|\to+\infty} \bar{\mathcal{L}}(v,\sigma^0,a^0) = +\infty, \qquad \lim_{\|(\sigma,a)^\top\|\to+\infty} \bar{\mathcal{L}}(v^0,\sigma,a) = -\infty \tag{80}$$

From Theorem 4.3.1 in (Hiriart-Urruty and Lemaréchal, 1993), the set of solutions of the saddle point problem (78) is a nonempty compact and convex set. The strict convexity of $\bar{\mathcal{L}}$ with respect to v for all $(\sigma, a) \in C$ and the strict concavity with respect with respect to σ, a for all v such that $H^\top v^0 + (\theta(1+e)-1)v_{\text{N},k} \geq 0$ imply the uniqueness of the solution of (78). To obtain a complete solution of (76) it suffices to compute $\dot{\varepsilon} = Bv$ and $\theta v_{\text{N}} = H^\top v - (1-\theta)v_{\text{N},k}$. □

Proposition 2. *Under Assumptions 1 and 2, the problem (75) has a solution for* $(v_{k+\theta}, \sigma_{k+\theta}, a_{k+\theta}, v_{\mathrm{N},k+1})$ *and* $(z_{k+\theta}, y_{k+\theta}, p_{\mathrm{N},k+1})$*. Furthermore, the solution is unique for* $(v_{k+\theta}, \sigma_{k+\theta}, a_{k+\theta}, v_{\mathrm{N},k+1}, z_{k+\theta}, y_{k+\theta})$*.*

As it is noted in (Hiriart-Urruty and Lemaréchal, 1993, Remark 4.3.2), the coercivity properties (80) imply that the following necessary optimality conditions has a solution

$$\begin{cases} 0 \in \partial_v \bar{\mathcal{L}}(v, \sigma, a) \\ 0 \in \partial_{\sigma,a} \bar{\mathcal{L}}(v, \sigma, a) \end{cases} \tag{81}$$

With our setting we get

$$\begin{aligned} (\partial_v \bar{\mathcal{L}}:) \qquad 0 &\in M(v - v_k) - h\theta f_{\mathrm{ext,k+1}}^{\top} + B^{\top}\lambda + \theta^2 H \partial \Psi_{\mathbb{R}_+^m}(H^{\top}v + (\theta(1+e)-1)v_{\mathrm{N},k}) \\ (\partial_\sigma \bar{\mathcal{L}}:) \qquad 0 &\in -S(\sigma - \sigma_k) + h\theta\dot{\varepsilon} - h\theta\partial_\sigma \Psi_C \begin{pmatrix} \sigma \\ a \end{pmatrix} \\ (\partial_a \bar{\mathcal{L}}:) \qquad 0 &\in -D^{-1}(a - a_k) - h\theta\partial_a \Psi_C \begin{pmatrix} \sigma \\ a \end{pmatrix} \end{aligned} \tag{82}$$

Let us introduce θv_{N} such that

$$\theta v_{\mathrm{N}} = H^{\top}v + (\theta(1+e)-1)v_{\mathrm{N},k}) \tag{83}$$

and z, y, p_{N}

$$-\begin{pmatrix} z \\ y \\ p_{\mathrm{N}} \end{pmatrix} \in \partial \Psi_{C \times \mathbb{R}_+^m} \begin{pmatrix} \sigma \\ a \\ v_{\mathrm{N}}. \end{pmatrix} \tag{84}$$

Then, the optimality conditions can be written as

$$\begin{cases} M(v - v_k) + h\theta B^{\top}\sigma = h\theta f_{\mathrm{ext,k+1}}^{\top} + \theta H p_{\mathrm{N}} \\ S(\sigma - \sigma_k) - h\theta B v = h\theta z \\ D^{-1}(a - a_k) = h\theta y \\ \theta v_{\mathrm{N}} = H^{\top}v - (1-\theta)v_{\mathrm{N},k} \\ -\begin{pmatrix} z \\ y \\ p_{\mathrm{N}} \end{pmatrix} \in \partial \Psi_{C \times \mathbb{R}_+^m} \begin{pmatrix} \sigma \\ a \\ v_{\mathrm{N}} + e v_{\mathrm{N},k} \end{pmatrix} \end{cases} \tag{85}$$

A solution of (85) is a solution of the problem (75). The uniqueness of $(v_{k+\theta}, \sigma_{k+\theta}, a_{k+\theta}, v_{\mathrm{N},k+1}, z_{k+\theta}, y_{k+\theta})$ is directly obtained from the Proposition 1. □

Remark 3. *The assumption on the positivity of the matrix* D *implies a positive hardening that prevents from softening behavior. In the case of perfect plasticity with* $D = 0$*, the variable* a *and the associated terms can be removed from the problem and we get the same results for existence and uniqueness of solutions of the discrete problem.*

The assumption on the velocity v^0 *in (77) is a standard assumption for the feasibility of the problem that can be found in a more general context of contact and friction in (V. Acary et al., 2011). Note that if* H *has full rank that condition is satisfied.*

In Appendix C, the optimality conditions for (76) are also equivalent to the problem (75).

Reduction of the linear equations Solving directly the problem (74) or the minimax problem (76) is possible with numerical methods of optimization, but, in the sequel, we prefer reduce the linear equations to reduce the number of unknown variables. The first three lines of (74) are linear equations and the discrete velocity v_{k+1} can be substituted to obtain a reduced variational inequality. Using the two first relations in (75), we obtain

$$h\theta z_{k+\theta} = S(\sigma_{k+\theta} - \sigma_k) - h\theta B\left(v_k + \theta M^{-1}\left(hf_{\text{ext,k}+\theta} + Hp_{\text{N},k+1} - hB^\top \sigma_{k+\theta}\right)\right), \tag{86}$$

that can be simplified in

$$h\theta z_{k+\theta} = \underbrace{\left[S + h^2\theta^2 BM^{-1}B^\top\right]}_{U}\sigma_{k+\theta} - \underbrace{\left[h\theta^2 BM^{-1}H\right]}_{V}p_{\text{N},k+1} + s, \tag{87}$$

with $s = -S\sigma_k - h\theta B\left(v_k + \theta hM^{-1}f_{\text{ext,k}+\theta}\right)$. A similar expression for $v_{\text{N},k+1} + ev_{\text{N},k}$ is obtained by mutliplying by $H^\top$:

$$v_{\text{N},k+1} + ev_{\text{N},k} = ev_{\text{N},k} + H^\top\left(v_k + h\theta M^{-1}f_{\text{ext,k}+\theta}\right) + H^\top M^{-1}Hp_{\text{N},k+1} - hH^\top M^{-1}B^\top\sigma_{k+\theta}. \tag{88}$$

In order to get a symmetric problem, we multiply the previous equation by θ^2

$$\theta^2(v_{\text{N},k+1} + ev_{\text{N},k}) = \underbrace{\theta^2 H^\top M^{-1}H}_{W}p_{\text{N},k+1} - \underbrace{h\theta^2 H^\top M^{-1}B^\top}_{V^\top}\sigma_{k+\theta} + r \tag{89}$$

with $r = \theta^2\left(ev_{\text{N},k} + H\left(v_k + \theta M^{-1}\left(hf_{\text{ext,k}+\theta}\right)\right)\right)$. The last line of the inclusion is finally rewritten as

$$h\theta y_{k+\theta} = D^{-1}(a_{k+\theta} - a_k). \tag{90}$$

Since the inclusion involves a cone, the problem (74) amounts to solving the following affine variational inequality

$$-\left(Q\begin{pmatrix}\sigma_{k+\theta}\\ a_{k+\theta}\\ p_{\text{N},k+1}\end{pmatrix} + p\right) \in N_{C\times\mathbb{R}^m_+}\begin{pmatrix}\sigma_{k+\theta}\\ a_{k+\theta}\\ p_{\text{N},k+1}\end{pmatrix}, \tag{91}$$

with

$$Q = \begin{pmatrix}U & 0 & -V\\ 0 & D^{-1} & 0\\ -V^\top & 0 & W\end{pmatrix} \text{ and } p = \begin{pmatrix}s\\ D^{-1}a_k\\ r\end{pmatrix}. \tag{92}$$

Equivalent convex quadratic optimization problem The goal of the section is to show that the affine variational inequality (91) is equivalent to a convex quadratic problem if Assumptions 1 hold. The matrix Q can be written as

$$\begin{aligned} Q &= \begin{pmatrix}S & 0 & 0\\ 0 & D^{-1} & 0\\ 0 & 0 & 0\end{pmatrix} + \begin{pmatrix}h^2\theta^2 BM^{-1}B^\top & 0 & -h\theta^2 BM^{-1}H\\ 0 & 0 & 0\\ -h\theta^2 H^\top M^{-1}B^\top & 0 & \theta^2 H^\top M^{-1}H\end{pmatrix}\\ &= \begin{pmatrix}S & 0 & 0\\ 0 & D^{-1} & 0\\ 0 & 0 & 0\end{pmatrix} + \begin{pmatrix}-h\theta B^\top & 0 & \theta H\end{pmatrix}^\top M^{-1}\begin{pmatrix}-h\theta B^\top & 0 & \theta H\end{pmatrix}. \end{aligned} \tag{93}$$

In this form, the matrix Q appears to be a symmetric semi-definite matrix as a sum of two symmetric semi-definite matrices. With this property, solving the affine variational inequality (91) is equivalent to solve the following convex quadratic optimization problem

$$\begin{aligned} \min_{\sigma,a,p_N} \quad & \frac{1}{2}\begin{pmatrix}\sigma\\ a\\ p_N\end{pmatrix}^\top Q \begin{pmatrix}\sigma\\ a\\ p_N\end{pmatrix} + p^\top \begin{pmatrix}\sigma\\ a\\ p_N\end{pmatrix} \\ \text{s.t.} \quad & \begin{pmatrix}\sigma\\ a\\ p_N\end{pmatrix} \in C \times \mathbb{R}^m_+. \end{aligned} \tag{94}$$

The well-posedness of the problem (94) is then equivalent of the well–posedness of the optimization problem. We already ensure that the solution exists and is unique except for p_N. In the convex case without strict convexity, results can be quite technical and needs assumption on the matrix H such as Slater condition. In the following paragraph, we prove it in the simpler case of strict convexity of the cost function adding a rank condition on H.

Existence and uniqueness in the strictly convex case. To prove the existence and uniqueness of solutions, let us define the following assumption.

Assumption 3. *The matrix H has full rank.*

Proposition 3. *Under Assumptions 1 and 3, the problem (94) has a unique solution (σ, a, p_N) if the set C is a non empty convex set for a sufficiently small time step.*

Under Assumptions 1 and 3, the matrix $W = \theta^2 H^\top M^{-1} H$ is a symmetric positive definite matrix. The matrix Q can be written as

$$Q = \begin{pmatrix} S & 0 & 0\\ 0 & D^{-1} & 0\\ 0 & 0 & W \end{pmatrix} + h \begin{pmatrix} h\theta^2 B M^{-1} B^\top & 0 & -\theta^2 B M^{-1} H\\ 0 & 0 & 0\\ -\theta^2 H^\top M^{-1} B^\top & 0 & 0 \end{pmatrix} \tag{95}$$

For a sufficiently small time step, the matrix Q is then a positive definite matrix. Since the optimization problem (94) is strictly convex, a unique solution exists if the C is a non-empty convex set. □

Remark 4. *This assumption 3 deserves some comments. The full rank property of the matrix H is standard in finite element application where the constraints are chosen to be linearly independent.*

3.4 Numerical methods

Since the problem (94) appears to be a convex quadratic optimization problem, numerous numerical methods can be applied to solve it. In practice, the set C is generally finitely represented and given by a set of inequalities that describes the yield function:

$$C = \{\sigma, a \mid f(\sigma, a) \geq 0\}. \tag{96}$$

where f is a smooth vector-valued function with non-vanishing gradients at the solution. The optimization problem (94) takes the form

$$\begin{aligned} \min_{\sigma,a,p_N} \quad & \tfrac{1}{2}\begin{pmatrix}\sigma\\ p_N\\ a\end{pmatrix}^\top Q \begin{pmatrix}\sigma\\ p_N\\ a\end{pmatrix} + p^\top \begin{pmatrix}\sigma\\ p_N\\ a\end{pmatrix} \\ \text{s.t.} \quad & f(\sigma, a) \geq 0 \\ & p_N \geq 0 \end{aligned} \tag{97}$$

that can be solved by any kind of numerical optimization techniques for solving quadratic optimization (Bonnans et al., 2006), interior point methods (Wright, 1996), semi-smooth Newton methods, proximal algorithms (Parikh, 2014) such as Alternating Direction Methods of Multipliers (ADMM). In the context of quasistatic plasticity, some of these methods have already been validated, see for instance (Kanno, 2020; Krabbenhøft et al., 2007; K. Krabbenhoft et al., 2007; Shimizu and Kanno, 2018) and also in the coupled problem of contact and plasticity (Christensen, 2002a). It may happen that C has the structure of a pointed convex cone. In this case, it is difficult to express the set C with a smooth vector-valued function, but most of the standard yield function in computational plasticity can be formulated on symmetric cone of semi-definite type or second order types (Berga and Géry De Saxcé, 1994; Bisbos et al., 2005; Hjiaj et al., 2003). Then the tools from second-order cone or semi-definite programming can be used.

The case of a feasible set C defined by linear relations When the set C is finite represented as in (96) and assuming that f is sufficiently smooth with nonvanishing gradients, the normal cone to C can expressed as

$$N_C \begin{pmatrix} \sigma \\ a \end{pmatrix} = \left\{ z, y \mid \begin{pmatrix} z \\ y \end{pmatrix} = -\nabla^\top_{\sigma,a} f(\sigma, a)\lambda, \lambda \geq 0, \lambda^\top f(\sigma, a) = 0 \right\}. \tag{98}$$

Then the plastic flow rule

$$\begin{pmatrix} \dot{\varepsilon}^p \\ -\dot{\alpha} \end{pmatrix} \in N_C \begin{pmatrix} \sigma \\ a \end{pmatrix} \tag{99}$$

is expressed as the classical flow rule for plasticity with the complementarity condition

$$\begin{cases} \dot{\varepsilon}^p = -\nabla^\top_\sigma f(\sigma, a)\lambda \\ \dot{\alpha} = \nabla^\top_a f(\sigma, a)\lambda \\ 0 \leq \lambda \perp f(\sigma, a) \geq 0, \end{cases} \tag{100}$$

where λ is the vector of plastic multipliers. If the yield function f is linear, the gradients are given by constant matrices denoted by

$$J_\sigma = \nabla^\top_\sigma f(\sigma, a) \quad \text{and} \quad J_a = \nabla^\top_a f(\sigma, a), \tag{101}$$

and we have

$$f(\sigma, a) = J^\top_\sigma \sigma + J^\top_a a + \kappa_Y. \tag{102}$$

With linear yield functions, the variational inequality (91) can be reduced to a Linear Complementarity Problem (LCP). To this aim, we express the stress tensor from (87) as

$$\sigma_{k+\theta} = h\theta U^{-1} J_\sigma \lambda - U^{-1} s + U^{-1} V p_{\mathrm{N},k+1}. \tag{103}$$

Substituting (103) in (89) and (102) yields

$$\theta^2 (v_{\mathrm{N},k+1} + e v_{\mathrm{N},k}) \quad = \quad (W - V^\top U^{-1} V) p_{\mathrm{N},k+1} - h\theta V^\top U^{-1} J_\sigma \lambda + V^\top U^{-1} s + r, \tag{104}$$

and

$$\begin{array}{rcl} f_{k+\theta} & = & J^\top_\sigma \sigma_{k+\theta} + J^\top_a a_{k+\theta} + \kappa_Y \\ & = & h\theta \left(J^\top_\sigma U^{-1} J_\sigma + J^\top_a D J_a \right) \lambda + J^\top_\sigma U^{-1} V p_{\mathrm{N},k+1} - J^\top_\sigma U^{-1} s + J^\top_a a_k + \kappa_Y. \end{array} \tag{105}$$

The problem in terms of λ and $p_{\mathrm{N},k+1}$ can be defined in the form of the follwing LCP

$$\begin{cases} \begin{pmatrix} f_{k+\theta} \\ v_{\mathrm{N},k+1} + e v_{\mathrm{N},k} \end{pmatrix} = L \begin{pmatrix} h\theta\lambda \\ p_{\mathrm{N},k+1} \end{pmatrix} + q \\ \\ 0 \leq h\theta\lambda \perp f_{k+\theta} \geq 0 \\ 0 \leq v_{\mathrm{N},k+1} + e v_{\mathrm{N},k} \perp p_{\mathrm{N},k+1}, \end{cases} \tag{106}$$

with

$$L = \begin{pmatrix} J_\sigma^\top U^{-1} J_\sigma + J_a^\top D J_a & J_\sigma^\top U^{-1} V \\ -V^\top U^{-1} J_\sigma & W - V^\top U^{-1} V \end{pmatrix} \quad \text{and} \quad q = \begin{pmatrix} -J_\sigma^\top U^{-1} s + J_a^\top a_k + \kappa_Y \\ V^\top U^{-1} s + r \end{pmatrix}. \tag{107}$$

In the case of quasistatic plasticity without contact conditions, a very similar formulation of the problem as a LCP can be found in (G. Maier, 1984).

Remark 5. *If the yield functions f are not linear, a possibility is to solve a sequence of linearized LCP iteratively in a Newton-Josephy algorithm for Nonlinear Complementarity Problems(NCP), or other NCP solvers (Vincent Acary and Brogliato, 2008; Facchinei and Pang, 2003). This can be an alternative strategy as using a nonlinear optimization solver.*

3.5 Structure preserving properties

In this section, we are interested in the structure preserving properties of the proposed time–stepping scheme, especially, the discrete energy balance of the scheme when plastic flow and unilateral contact occur. In the continuous time and space setting the energy balance reads as:

$$\frac{d}{dt}\mathcal{E}(t) = \frac{d}{dt}(\mathcal{T}(t) + \Psi(t)) = -\mathcal{D}(t) + \mathcal{P}_{\mathrm{v}}(t) + \mathcal{P}_{\mathrm{ext}}(t), \tag{108}$$

where $\mathcal{E}(t)$ is total mechanical energy $\mathcal{E}(t) = \mathcal{T}(t) + \Psi(t)$. After the space discretization by a finite element method, the energy balance takes the form

$$\mathrm{d}(\mathsf{T}(t) + \Psi(t)) = -\mathsf{D}(t)\mathrm{d}t + \mathsf{P}_{\mathrm{ext}}(t)\mathrm{d}t + \mathrm{d}\mathsf{P}_{\mathrm{impact}}, \tag{109}$$

where the space-discretized energies are given by

$$\mathsf{E}(t) = \mathsf{T}(t) + \Psi(t) \quad \text{with } \mathsf{T}(t) = \frac{1}{2} v^\top(t) M v(t), \quad \text{and } \Psi(t) = \frac{1}{2} \varepsilon^{e\top}(t) E \varepsilon^e(t) + \frac{1}{2} \alpha^\top(t) D \alpha(t) \tag{110}$$

with the convention that the kinetic energy is also a right continuous function of bounded variations, *i.e*, $\mathsf{T}(t) = \mathsf{T}^+(t)$. The dissipation and the power of external forces are

$$\mathsf{D}(t) = \sigma^\top(t)\dot{\varepsilon}^p(t) - a^\top(t)\dot{\alpha}(t) \text{ and } \mathsf{P}_{\mathrm{ext}}(t) = f_{\mathrm{ext}}^\top(t) v(t). \tag{111}$$

Since in a discrete system, impacts may occur, the power of the reaction impulse is given by

$$\mathrm{d}\mathsf{P}_{\mathrm{impact}} = \frac{1}{2}(v_{\mathrm{N}}^+ + v_{\mathrm{N}}^-)\mathrm{d}i_{\mathrm{N}}. \tag{112}$$

Let us now compute the variation of the total mechanical energy over a time–step, starting by the kinetic energy

$$\Delta\mathsf{T}_k^{k+1} = \mathsf{T}(t_{k+1}) - \mathsf{T}(t_k) = \frac{1}{2}(v_{k+1} + v_k)^\top M (v_{k+1} - v_k). \tag{113}$$

Using the relation $\frac{1}{2}(v_{k+1} + v_k) = \frac{1}{h}(u_{k+1} - u_k) + (\frac{1}{2} - \theta)(v_{k+1} - v_k)$ and the first equation in (74), we obtain

$$\begin{aligned} \Delta\mathsf{T}_k^{k+1} &= (\tfrac{1}{2} - \theta)\|v_{k+1} - v_k\|_M + v_{k+\theta}^\top \left(h f_{\mathrm{ext,k}+\theta} - hB^\top \sigma_{k+\theta} + H p_{\mathrm{N},k+1}\right) \\ &= (\tfrac{1}{2} - \theta)\|v_{k+1} - v_k\|_M + h v_{k+\theta}^\top f_{\mathrm{ext,k}+\theta} - h\sigma_{k+\theta}^\top \dot{\varepsilon}_{k+\theta} + v_{\mathrm{N},k+\theta}^\top p_{\mathrm{N},k+1}. \end{aligned} \tag{114}$$

For the potential energy, we obtain

$$\begin{aligned}\Delta\Psi_k^{k+1} &= \Psi(t_{k+1}) - \Psi(t_k) = \tfrac{1}{2}(\varepsilon_{k+1}^e + \varepsilon_k^e)^\top E(\varepsilon_{k+1}^e - \varepsilon_k^e) + \tfrac{1}{2}(\alpha_{k+1} + \alpha_k)^\top D(\alpha_{k+1} - \alpha_k) \\ &= (\tfrac{1}{2} - \theta)\|\varepsilon_{k+1}^e - \varepsilon_k^e\|_E + h\sigma_{k+\theta}^\top \dot{\varepsilon}_{k+\theta}^e + (\tfrac{1}{2} - \theta)\|\alpha_{k+1} - \alpha_k\|_D + h y_{k+\theta}^\top \alpha_{k+\theta}.\end{aligned} \tag{115}$$

Using the approximation of works of external forces and the dissipated work by the θ-method as

$$\mathsf{W}_{\text{ext}\ k}^{k+1} := h v_{k+\theta}^\top f_{\text{ext,k}+\theta} \approx \int_{t_k}^{t_{k+1}} \mathsf{P}_{\text{ext}}(t)\mathrm{d}t, \tag{116}$$

and

$$\mathsf{W}_{p\ k}^{k+1} := h\sigma_{k+\theta}^\top \dot{\varepsilon}_{k+\theta}^p - h a_{k+\theta}^\top y_{k+\theta} \approx \int_{t_k}^{t_{k+1}} \mathsf{D}(t)\mathrm{d}t, \tag{117}$$

and finally, an approximation of the work dissipated by the percussion (see (Vincent Acary, 2016))

$$\mathsf{W}_{c\ k}^{k+1} := v_{\text{N},k+\theta}^\top p_{\text{N},k+1} = (1 - \theta(1+e))v_{\text{N},k}^\top p_{\text{N},k+1}, \tag{118}$$

the increment of total energy is then given by

$$\Delta\mathsf{E}_k^{k+1} - \mathsf{W}_{\text{ext}\ k}^{k+1} + \mathsf{W}_{p\ k}^{k+1} - \mathsf{W}_{c\ k}^{k+1} = (\frac{1}{2} - \theta)\left(\|v_{k+1} - v_k\|_M + \|\varepsilon_{k+1}^e - \varepsilon_k^e\|_E + \|\alpha_{k+1} - \alpha_k\|_D\right). \tag{119}$$

The following proposition summarizes the properties of the discrete energy balance (119).

Proposition 4. *The main conclusions that can be drawn for the energy/dissipation of the scheme are*

1. *For $\theta = \dfrac{1}{2}$, the time–stepping scheme satisfies the approximation of the discrete energy balance without introducing artificial dissipation:*

$$\Delta\mathsf{E}_k^{k+1} - \mathsf{W}_{\text{ext}\ k}^{k+1} = -\mathsf{W}_{p\ k}^{k+1} + \mathsf{W}_{c\ k}^{k+1}. \tag{120}$$

2. *The dissipated work due to plasticity is positive and for $\theta \leq \dfrac{1}{1+e}$, the dissipated work due to impact is also positive.*

3. *For $\dfrac{1}{2} \leq \theta \leq \dfrac{1}{1+e} \leq 1$, we have the following dissipation inequality*

$$\Delta\mathsf{E}_k^{k+1} - \mathsf{W}_{\text{ext}\ k}^{k+1} \leq 0. \tag{121}$$

A result in (Vincent Acary, 2016) shows that

$$\mathsf{W}_{c\ k}^{k+1} \leq 0 \text{ for } \theta \leq \frac{1}{1+e}. \tag{122}$$

Furthermore, the inclusion

$$-\begin{pmatrix} z_{k+\theta} \\ y_{k+\theta} \end{pmatrix} \in N_{C\times\mathbb{R}_+^m}\begin{pmatrix} \sigma_{k+\theta} \\ a_{k+\theta} \end{pmatrix}, \tag{123}$$

implies that $\mathsf{W}_p \geq 0$. □

Remark 6. *This inequality* (121) *ensures the practical unconditional stability of the scheme.*

4 Numerical applications

In this section, a series of examples demonstrates the capabilities of the formulation proposed. The choice was made to focus on beam structures able to sustain both tensile and bending forces. Assuming that plastic strains occur from the combined effects of axial and bending forces, we considered a yield surface expressed in terms of tensile and bending stresses. Associated flow rule as well as isotropic and kinematic hardening were considered. Both the statics and dynamics responses of the structures were analyzed. Dedicated Python scripts were developed using the LCPs solvers implemented in Siconos code (Vincent Acary, Bonnefon, et al., 2019).

4.1 Finite element model of elastoplastic beam structures

4.1.1 Finite element method for Elasto-plastic Euler-Bernoulli beam.

In the examples, specific beam elements able to sustain bending and tensile loadings are used. Beam elements based on Euler–Bernoulli beam theory are classically formulated using third order shape functions and numerical integration techniques based on Gaussian quadrature that involve two Gauss points per element. In order to consider two Gauss points for the axial displacements, we introduced elements with three nodes and quadratic shape functions in the axial direction. The nodal displacements and Gauss point locations of the element used are presented in Figure 1.

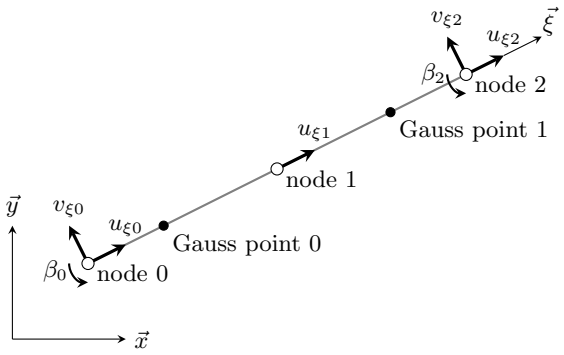

Figure 1: Description of the beam element used

For each element, the generalized stresses are expressed at Gauss points as :

$$\sigma_e = [n_1 \quad m_1 \quad n_2 \quad m_2]^\top, \tag{124}$$

where n_i is the normal force at Gauss point i and m_i is the bending moment at Gauss point i. Standard elementary matrices are recalled in Appendix B.

4.1.2 Linear yield surface

The chosen plastic yield surface takes into account the combined effects of axial and bending forces when a plastic flow occurs. A yield criterion based on the approach proposed in P. Heng et al. (2016) and Duan and W.-F. Chen (1990) is chosen, in the specific case of linear yield functions (see Figure 2). Using the notation introduced in Section 3.4 for a set of linear yield criteria, the matrices $J_\sigma^\top$, $J_a^\top$, κ_Y are defined

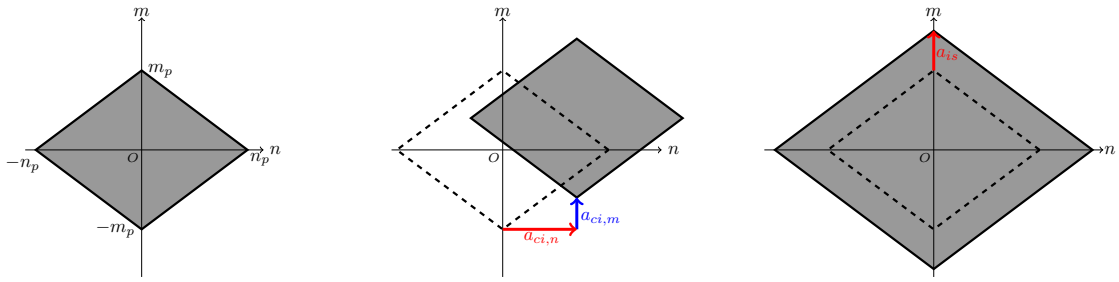

(a) Perfect plasticity (b) Kinematic hardening (c) Isotropic hardening

Figure 2: Yield surface in the case of perfect plasticity (a), kinematic hardening (b), and isotropic hardening (c) in the space of generalized stresses (n, m).

in the present case by

$$J_\sigma^\top = \begin{bmatrix} -\frac{1}{n_p} & -\frac{1}{m_p} \\ \frac{1}{n_p} & -\frac{1}{m_p} \\ \frac{1}{n_p} & \frac{1}{m_p} \\ -\frac{1}{n_p} & \frac{1}{m_p} \end{bmatrix}, \quad J_a^\top = \begin{bmatrix} \frac{1}{m_p} & \frac{1}{m_p} & \frac{1}{m_p} \\ -\frac{1}{m_p} & \frac{1}{m_p} & \frac{1}{m_p} \\ -\frac{1}{m_p} & -\frac{1}{m_p} & \frac{1}{m_p} \\ \frac{1}{m_p} & -\frac{1}{m_p} & \frac{1}{m_p} \end{bmatrix}, \quad \kappa_Y = \begin{bmatrix} 1 \\ 1 \\ 1 \\ 1 \end{bmatrix}, \tag{125}$$

where n_p is the limit admissible tensile force and m_p is the limit admissible bending moment. Both kinematic and isotropic hardenings are considered leading the definition of the force vector a, expressed at each Gauss point as

$$a = [a_{ki,n} \quad a_{ki,m} \quad a_{is}]^\top, \tag{126}$$

where $a_{ki,n}$ and $a_{ki,m}$ are associated with kinematic hardening in terms of normal force n and bending moment m, respectively and $a_{is} \geqslant 0$ is associated with isotropic hardening. The vector of plastic multipliers λ_i at Gauss point i is denoded by

$$\lambda_i = [\lambda_{i,1} \quad \lambda_{i,2} \quad \lambda_{i,3} \quad \lambda_{i,4}]^\top. \tag{127}$$

4.2 Example 1 : Cantilever beam subjected to quasi-static displacements

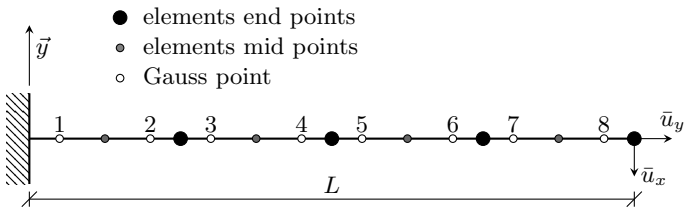

Figure 3: Example 1: Cantilever beam discretized in 4 elements subjected to quasi-static displacements $\bar{u}_x$ and $\bar{u}_y$ at its free end.

The first example is dedicated to evaluate the capability of the approach to simulate the response of elastoplastic structures subjected to various quasi-static loading scenarios. This example also illustrates the evolution of the different variables, in particular of the plastic multipliers, during the onset of plastic strains. The structure is an elastoplastic cantilever beam of length L, discretized in 4 beam elements to

L (m)	0.8	I (m^4)	0.0283×10^{-6}
A (m^2)	0.22×10^{-3}	E (MPa)	210 000
H_{ki} (MPa)	$E/10 = 21\,000 \times 10^6$	H_{is} (MPa)	$E/100 = 2100 \times 10^6$
n_P (N)	33 000	m_P (Nm)	283.5
ρ (kg/m^3)	7701		

Table 1: Properties of the elastoplastic cantilever beam used in example 1.

keep it as simple as possible, and subjected to quasi-static displacements $\bar{u}_x$ and $\bar{u}_y$ at its free end. The properties of the structure are summarized in Table 1.

As the formulation explicitly integrates dynamical effects, we can directly model the quasi-static loadings as low velocity dynamical loadings. To ensure a maximal dissipation of the kinetic energy, we used $\theta = 1$. Three cases are considered with different combinations of applied velocities and plastic behavior in order to reach different regimes for the plastic flows (see Figure 4 for a definition of the applied velocities).

- **Case 1** We consider a plastic law without hardening and a constant velocity is applied at the the beam free end. The axial and transversal components of the velocity are 1×10^{-4} m/s and 4×10^{-3} m/s , respectively (see Figure 4).
- **Case 2** We consider a plastic law with isotropic and kinematic hardening with the same prescribed velocities.
- **Case 3** In this case, we consider a plastic law with isotropic and kinematic hardening and we apply first a constant transversal velocity, set at 8×10^{-3} m/s until $t = 2.5$ s. Then, the transversal velocity is cancelled and a constant axial velocity, equal to 2×10^{-4} m/s, is applied (see Figure 4).

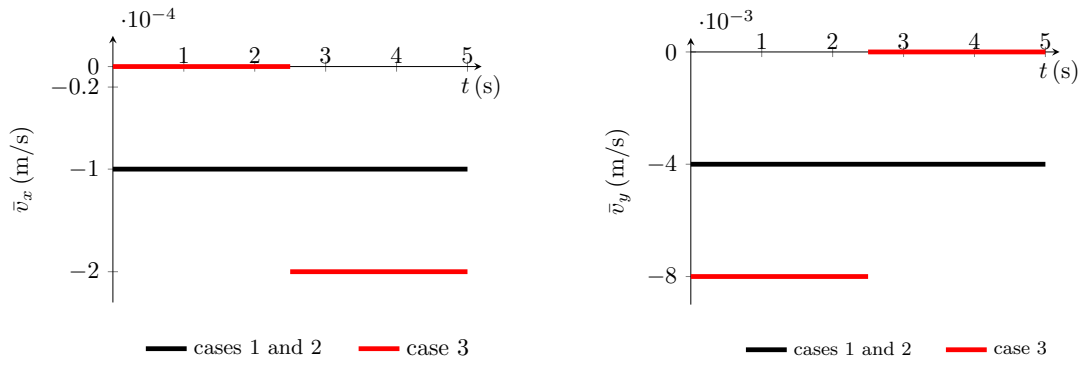

(a) axial velocity

(b) transversal velocity

Figure 4: Example 1: Time evolution of the applied velocities at the free extremity for the different loading cases.

Case 1: Transversal and axial displacement - perfect plasticity As shown in Figure 5, the axial force n_i and the bending moment m_i first linearly increase until the yield criterion is reached for Gauss point 1 at time $1.84\ s$. Once the yield criterion is reached, the plastic multiplier $\lambda_{1,3}$ becomes positive (Figure 7). Hence, the generalized stresses at Gauss point 1 evolve along the yield surface for increasing displacements (Figure 6). The onset of plastic strains at Gauss point 1 entails changes in the evolution of the stresses at all Gauss points. In particular, the bending moments decrease due to the formation of a plastic hinge at Gauss point 1.

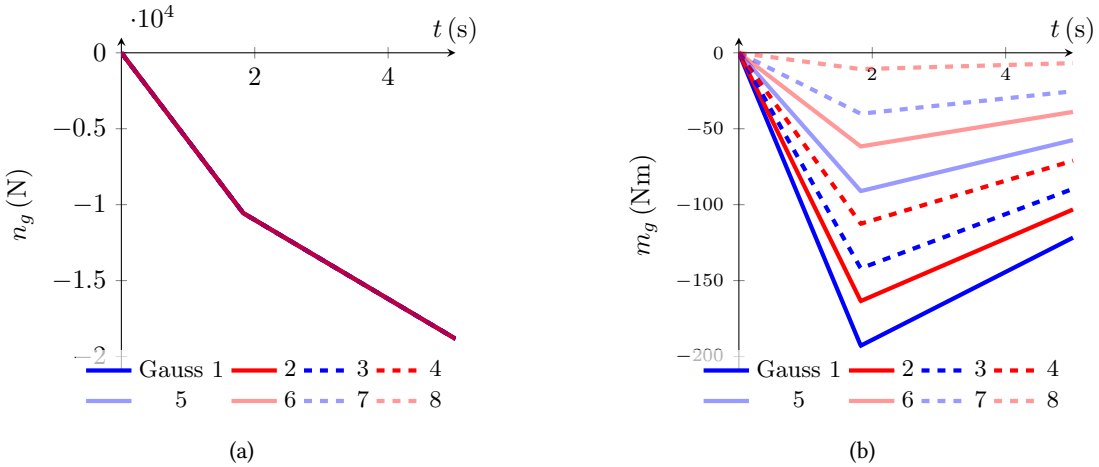

(a) (b)

Figure 5: Example 1, case1: time evolutions of the axial forces n_g (a) and bending moments m_g (b) at the Gauss points g of a cantilever beam subjected to axial and transversal displacements simultaneously in the case of perfect plasticity.

Case 2: Transversal and axial displacement - isotropic and kinematic hardening The introduction of hardening entails both translation of the yield surface and increase in this surface once the yield criterion is reached (Figure 9). Contrary to the case of perfect plasticity, the bending moments do not decrease when the yield criterion is reached (Figure 8). In this case, we do not observe a plastic hinge located only at Gauss point 1. The yield criterion is successively reached at Gauss point 2, and then at Gauss point 3, for increasing displacements. The plastic multipliers successively become positive (Figure 10) when the yield criterion is reached at a given Gauss point.

Case 3: Transversal followed by axial displacement - perfect plasticity The third case illustrates the specific situation when the stress at a Gauss point reaches a corner of the admissible set, i.e. an intersection of two linear limits of the yield surface. The node displacements are depicted in Figure 11. When the yield criterion is reached at Gauss point 1 for $t = 1.4\ s$ (Figure 13a), the plastic multipliers $\lambda_{1,3}$ and $\lambda_{1,4}$ both become positive (Figure 14). Indeed, at the corner, the yield criterion fullfillment requires the activation of two conditions. The onset of plastic strains results in the formation of a plastic hinge at Gauss point 1. As classically for perfectly plastic cantilever beams subjected to bending loading only, the bending moments remain constant when the yield criterion is reached (Figure 12). When the transversal velocity is cancelled and the constant axial velocity is applied ($t = 2.5$ s - Figure 11), the loading path is modified. Thus, only one inequality constraint is active and the multiplier $\lambda_{1,4}$ vanishes (Figure 14). To fullfill the yield criterion under this loading path, the bending moments decrease while the axial forces increase (Figure 12).

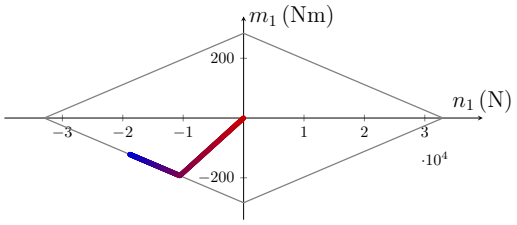

(a) Gauss point 1

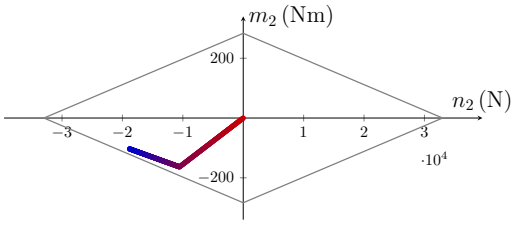

(b) Gauss point 2

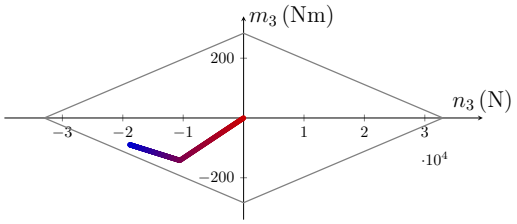

(c) Gauss point 3

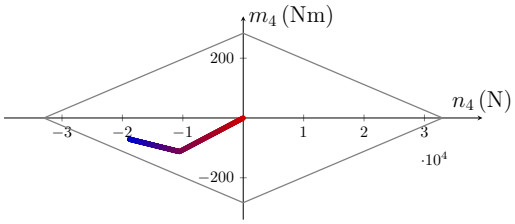

(d) Gauss point 4

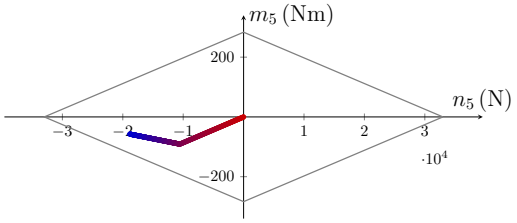

(e) Gauss point 5

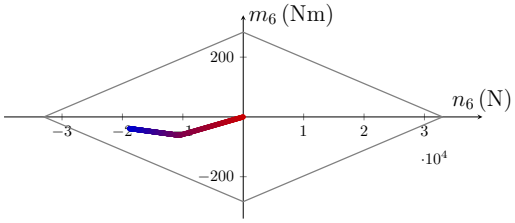

(f) Gauss point 6

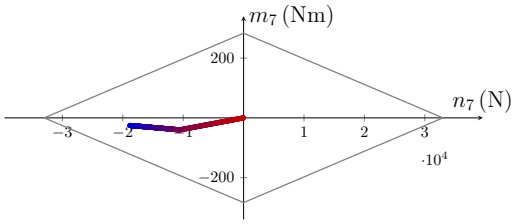

(g) Gauss point 7

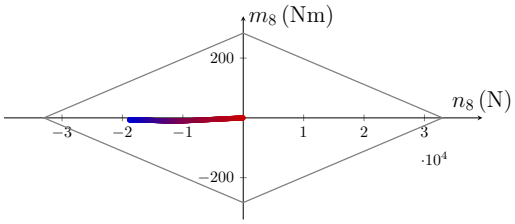

(h) Gauss point 8

Figure 6: Example 1, case 1: stress path at the Gauss points of the cantilever beam subjected to axial and transversal displacements simultaneously in the case of perfect plasticity. The bending moments m_g at the Gauss points g are plotted against the axial force n_g. The diamond shape is the yield surface C.

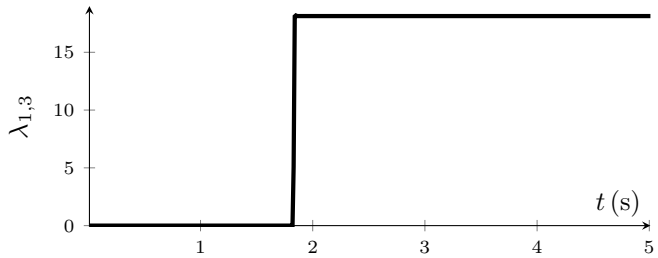

Figure 7: Example 1, case 1: time evolution of the plastic multipliers $\lambda_{1,3}$ at Gauss point 1 of the cantilever beam subjected to axial and transversal displacements simultaneously in the case of perfect plasticity.

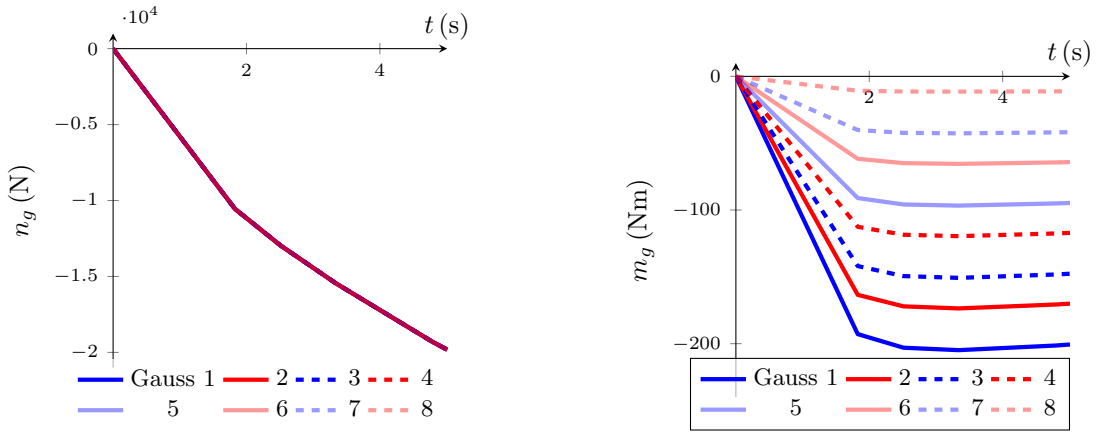

(a) (b)

Figure 8: Example 1, case 2: Time evolution of the axial forces n_g (a) and bending moments m_g (b) at the Gauss points g of the cantilever beam subjected to axial and transversal displacements simultaneously in the case of isotropic and kinematic hardenings.

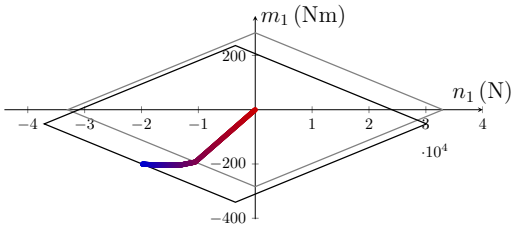

(a) Gauss point 1

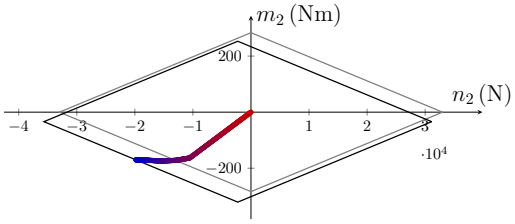

(b) Gauss point 2

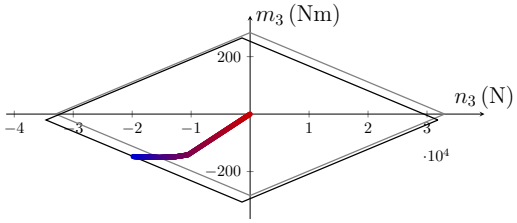

(c) Gauss point 3

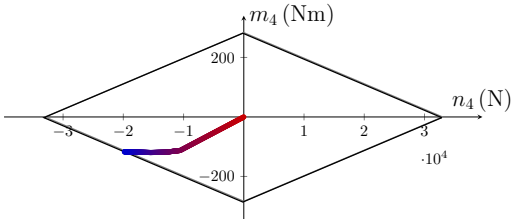

(d) Gauss point 4

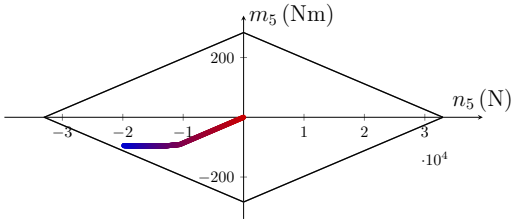

(e) Gauss point 5

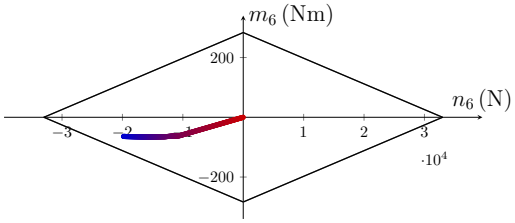

(f) Gauss point 6

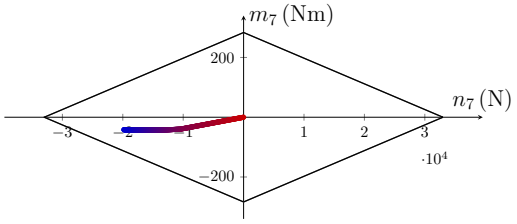

(g) Gauss point 7

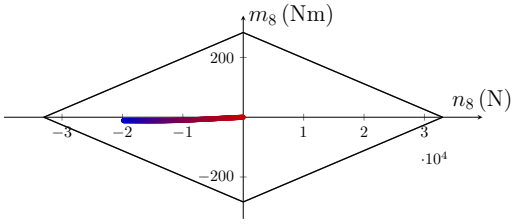

(h) Gauss point 8

Figure 9: Example 1, case 2: stress path at the Gauss points of the cantilever beam subjected to axial and transversal displacements simultaneously in the case of isotropic and kinematic hardenings. The bending moments m_g at the Gauss points g are plotted against the axial force n_g. The grey diamond shape is the initial yield surface and the black diamond shape is the final one.

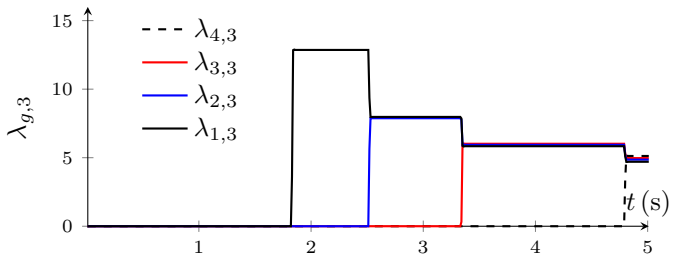

Figure 10: Example 1, case 2: time evolutions of the plastic multipliers $\lambda_{g,3}$ at the first 4 Gauss points g of the cantilever beam subjected to axial and transversal displacements simultaneously in the case of isotropic and kinematic hardening.

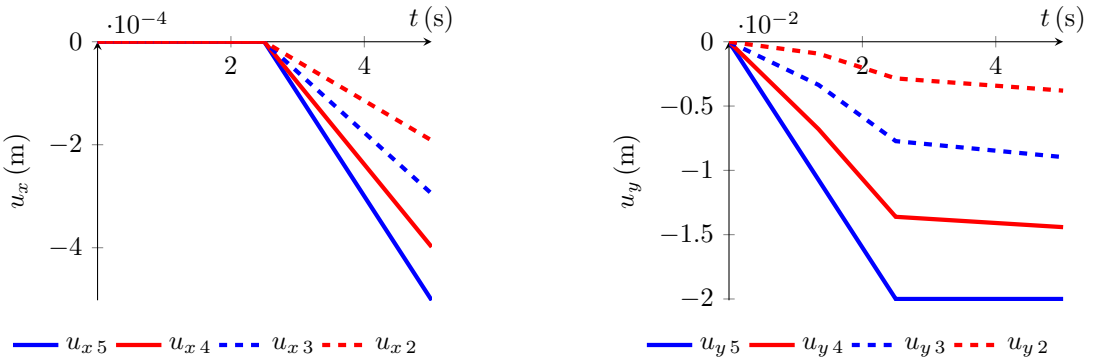

(a) axial displacement

(b) transversal displacement

Figure 11: Example 1, case 3: time evolution of the axial displacements u_x and transversal displacements u_y at the 4 free nodes of the cantilever beam successively subjected to transversal and axial displacements in the case of perfect plasticity.

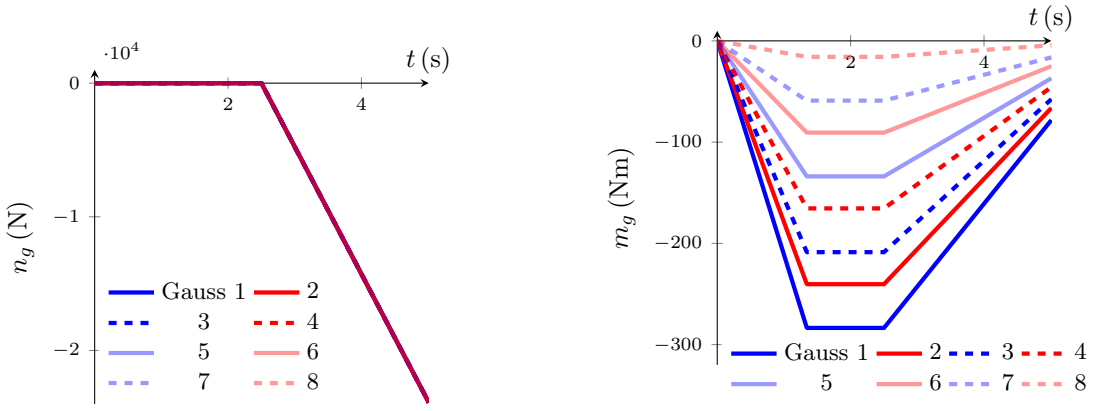

(a)

(b)

Figure 12: Example 1, case 3: Time evolution of the axial forces n_g (a) and bending moments m_g (b) at the Gauss points of the cantilever beam successively subjected to transversal and axial displacements in the case of perfect plasticity.

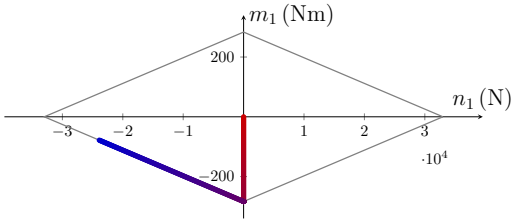

(a) Gauss point 1

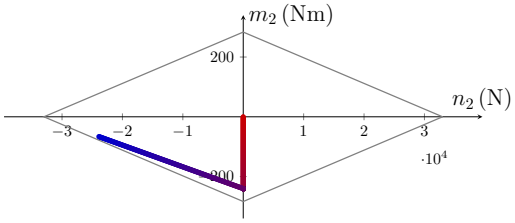

(b) Gauss point 2

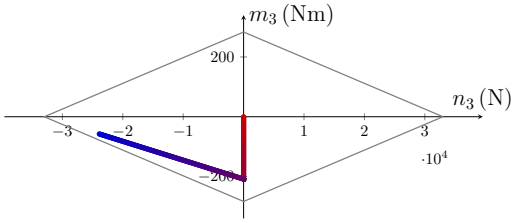

(c) Gauss point 3

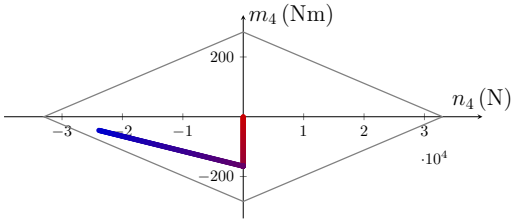

(d) Gauss point 4

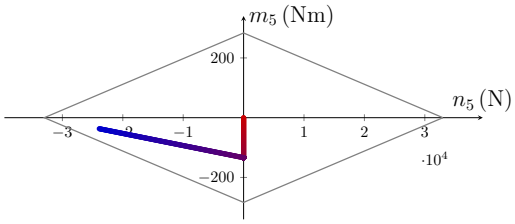

(e) Gauss point 5

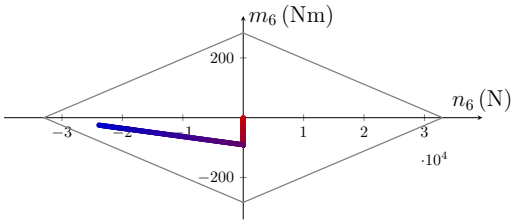

(f) Gauss point 6

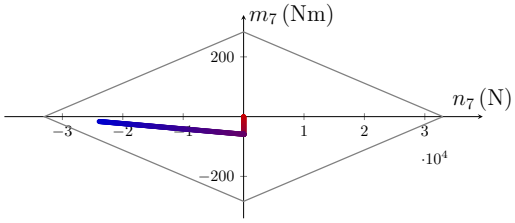

(g) Gauss point 7

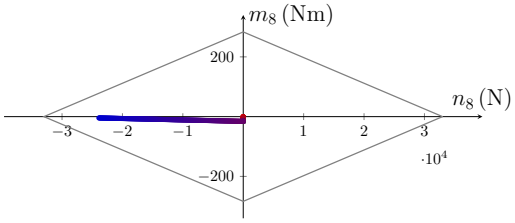

(h) Gauss point 8

Figure 13: Example 1, case 3: stress path at the Gauss points of the cantilever beam successively subjected to transversal and then axial displacements. The bending moments m_g at the Gauss points g are plotted against the axial force n_g. The diamond shape is the yield surface.

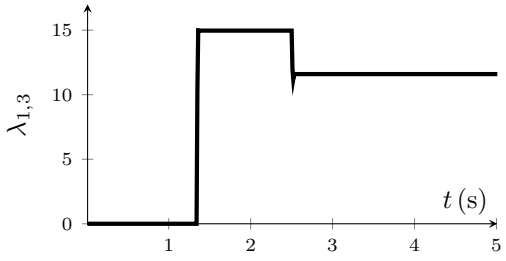

(a) $\lambda_{1,3}$

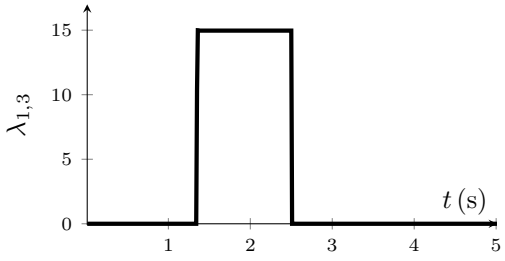

(b) $\lambda_{1,4}$

Figure 14: Example 1, case 3: time evolution of the plastic multipliers $\lambda_{1,3}$ (a) and $\lambda_{1,4}$ (b) at Gauss point 1 of the cantilever beam successively subjected to transversal and then axial displacements in the case of perfect plasticity.

4.3 Example 2 : Cantilever beam subjected to impact

The second example illustrates the relevance of the formulation for the joint assessment of plasticity and impact in a monolithic algorithm. The analysis focuses on the energy balance of the system, with specific interest on the evolution of energy dissipation depending on the parameters of the numerical scheme (time discretization, space discretization, and θ parameter).

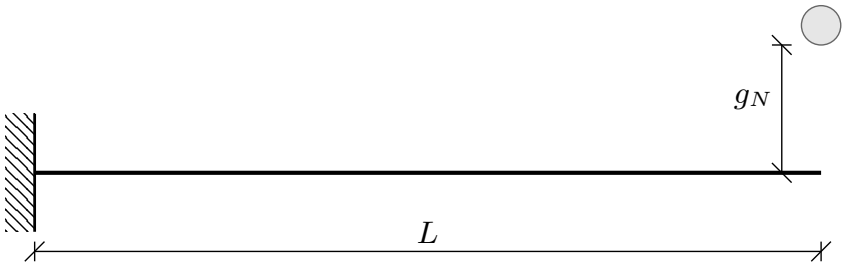

Figure 15: Example 2: impacted cantilever beam.

In this example, a elasto-plastic cantilever beam of length $L = 3\text{m}$, with isotropic and kinematic hardening, discretized with $n_{el} = 100$ elements, is impacted at its free end by a spherical projectile of mass m_{sphere}, initially located at a distance $q_{y\ sphere} = g_N(t = 0) = 1\text{m}$ (Figure 15). The properties of the beam and of the projectile are summarized in Table 2. The restitution coefficient was set at $e = 0$ to emphasize energy dissipation due to impact, θ was set at $1/2$ to prevent artificial energy dissipation and the time step was set at $h = 10^{-4}\text{s}$.

A (m^2)	3.4×10^{-3}	I (m^4)	8.643×10^{-6}
E (MPa)	210 000	ρ (kg/m^3)	7701
H_{ki} (MPa)	$E/10 = 21\,000$	H_{is} (MPa)	$E/100 = 2100$
n_P (N)	799 000	m_P (Nm)	33 840
m_{sphere} (kg)	250	$q_{y\ sphere}(t = 0)$ (m)	1
e	0		

Table 2: Example 2: properties of the cantilever beam and of the projectile.

The impact is first characterized by a succession of short interactions between the projectile and the beam (Figure 19 - light blue zone). As the restitution coefficient e is equal to 0, each interaction lasts few timesteps. The existence and the duration of this transient phase is also related with the stiffness of the beam, and the hich frequency dynamics generated by the FEM discretization. This phase is followed by a longer phase of permanent contact between the beam and the sphere (Figure 19 - blue zone). During this phase, the relative velocity vanishes while the impulse is always positive (Figure 19), as specified in the complementarity condition.

The impulses applied to the beam and to the projectile during the interaction induce the bouncing of the sphere and the bending of the beam (Figure 16). After the bouncing of the sphere, the undamped vibration of the beam is observed until a second impact. The beam oscillates around a negative equilibrium position since plastic strains developed during the first interaction phase.

Energy transfer In Figure 17, the discrete work of external forces $\mathsf{W}_{ext\ 0}^{\ k+1}$, i.e. the sum of the kinetic energy T_{k+1} and the free energy Ψ_{k+1}, is always equal to the sum of elastic mechanical energy E_{k+1}, plastic dissipation $\mathsf{W}_{p\ 0}^{\ k+1}$ and contact dissipation $\mathsf{W}_{c\ 0}^{\ k+1}$. Indeed, setting $\theta = 1/2$ prevents artificial energy dissipation. Just before impact, the work of external forces $\mathsf{W}_{ext\ 0}^{\ k+1}$ is equal to the kinetic energy of the sphere. During the simulation, $\mathsf{W}_{ext\ 0}^{\ k+1}$ varies depending on the vertical position of the sphere only (for the sake of clarity, gravity was not applied to the beam in this example). The first interaction between the sphere and the beam results in substantial energy dissipation (Figure 18), due to plastic flow

($\mathsf{W}_{p\ 0}^{k+1}$) and to contact ($\mathsf{W}_{c\ 0}^{k+1}$), to a lesser extent, until a permanent contact establishes between the sphere and the beam (Figure 16 - blue colored area). Then, as the relative velocities of the beam and the sphere at the contact point are equal, $\mathsf{W}_{c\ 0}^{k+1}$ remains constant while $\mathsf{W}_{p\ 0}^{k+1}$ still increases until the sphere reaches its lower position (Figure 18). Just before the end of the first interaction, a second transition period occurs, with activation and desactivation of the contact, associated to very small energy dissipation at contact as the relative velocities are very small. The same energy dissipation process occurs for the second interaction with substantially smaller energy dissipation. Between the two interaction phases, no energy dissipation occurs, as $\theta = 1/2$.

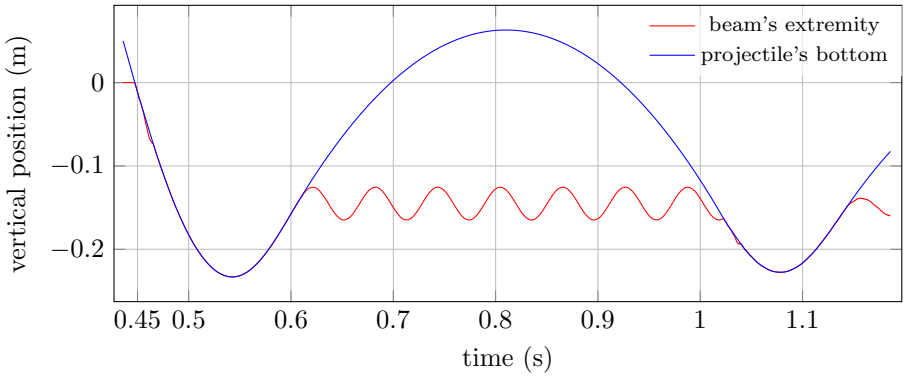

Figure 16: Example 2: vertical positions of the beam free end and sphere along time.

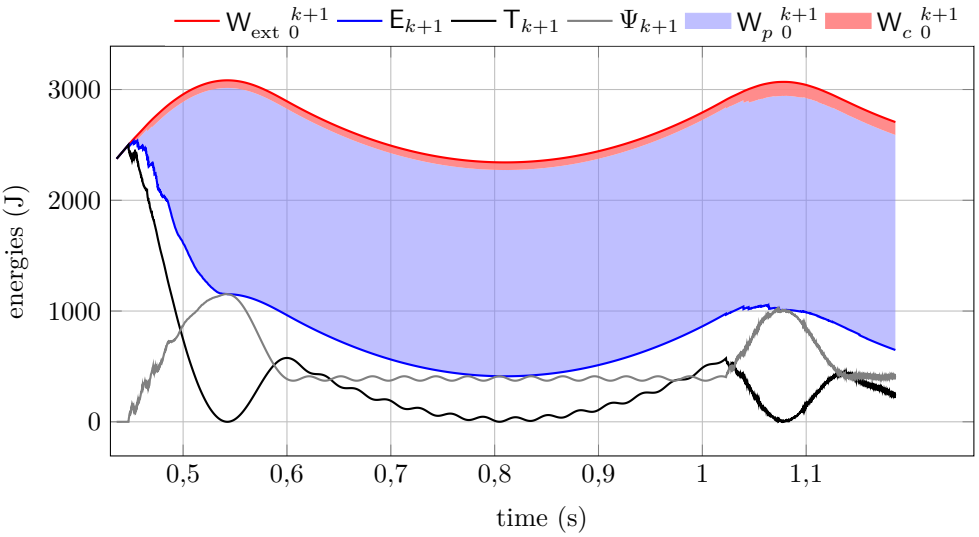

Figure 17: Time evolutions of the different energies and works involved in the impact of a cantilever beam by a sphere. The work of external forces $\mathsf{W}_{ext\ 0}^{k+1}$ is equal to the sum of mechanical energy E_{k+1}, plastic dissipation $\mathsf{W}_{p\ 0}^{k+1}$ and contact dissipation $\mathsf{W}_{c\ 0}^{k+1}$. And the elastic energy E_{k+1} is the sum of the kinetic energy T_{k+1} and the free energy Ψ_{k+1}

.

Time and space discretization To illustrate the influence of the time and space discretization on the discrete energy balance, we consider the first period from $t = 0\,\text{s}$ to $t = 0.457\,\text{s}$. As illustrated for the dissipation (Figure 20), energy dissipations due to plastic flow and contact tend to converge to a given value for refined time and space discretizations, i.e. increasing numbers of elements and decreasing time

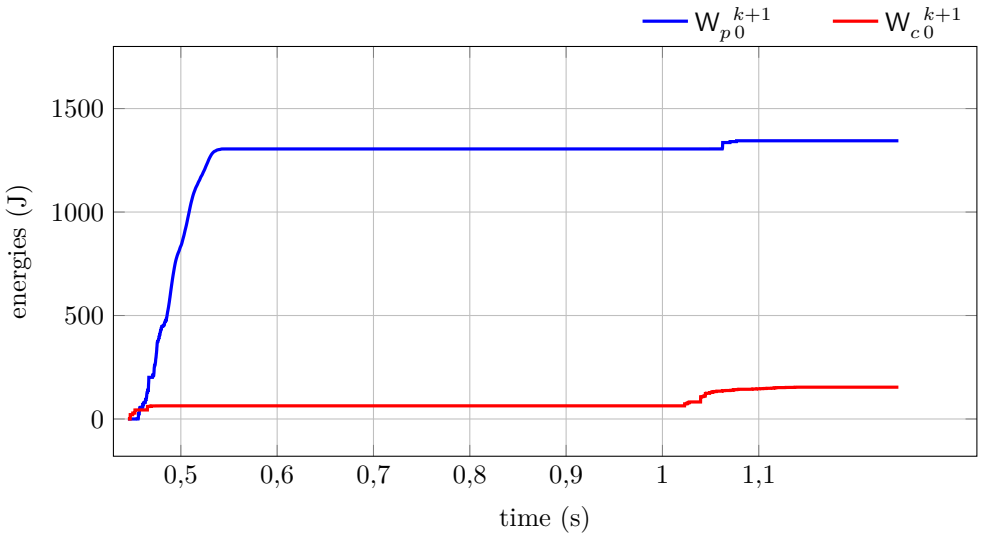

Figure 18: Time evolutions of the energies dissipated by plastic flow ($W_{p\,0}^{k+1}$) and contact ($W_{c\,0}^{k+1}$) during the impact of a sphere on a cantilever beam.

steps. A focus on the first percussion between the sphere and the beam (Figure 21) shows that convergence towards a threshold value of p_{N} is reached for any spatial resolution. In addition, smaller time steps are necessary to reach convergence for finer spatial discretizations. The threshold value of p_{N} depends on the spatial discretization : it decreases for increasing numbers of elements. This observation can be related to the open scientific question of the existence of percussion in this configuration for continuous beam (see Chatterjee (2004)). In this particular case, it seems that the percussion p_n vanishes with the time-step and the mesh size. It also questions the relevance of the energy dissipation at contact in practice on such an application.

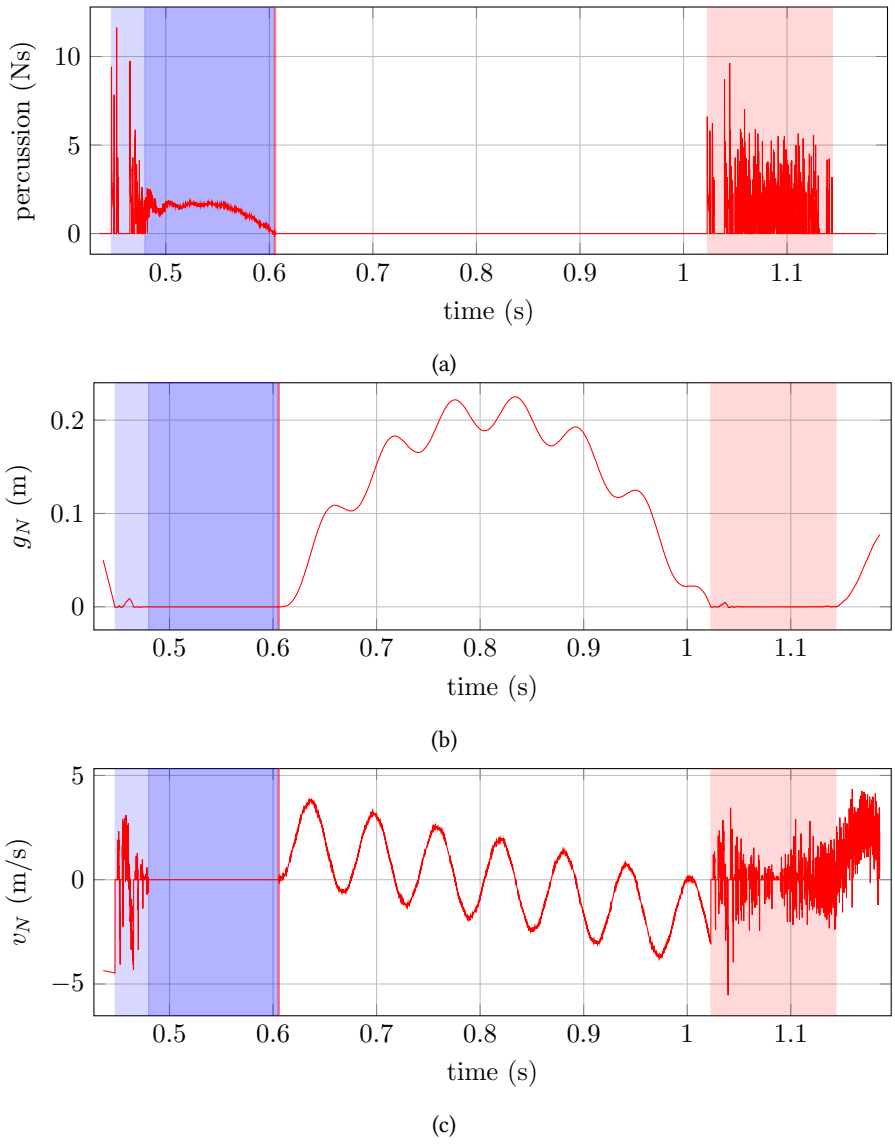

Figure 19: Example 2: Time evolutions of the reaction impulse (p_N), gap function (g_N) and relative normal velocity (v_N) during the impact of a sphere on a cantilever beam. We can observe a contact activation period where several contact activation are observed as in the first colored area (light blue), before a permanent contact occurs (second colored area - blue).

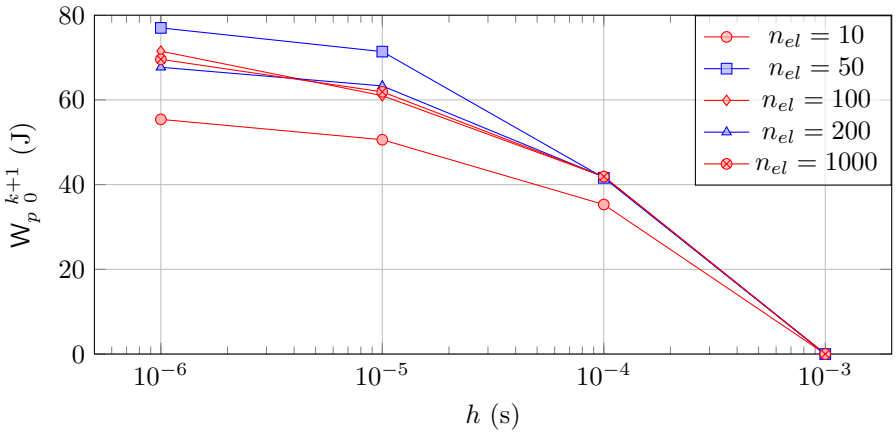

(a) Plastic dissipation

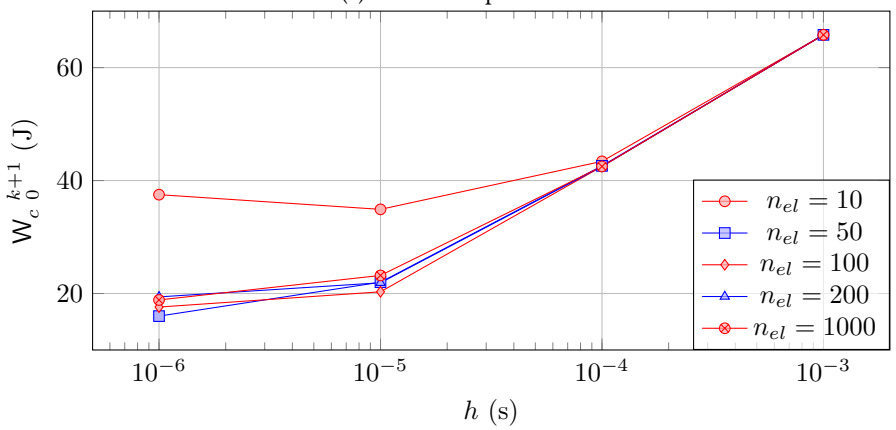

(b) Contact dissipation

Figure 20: Example 2: Convergence of the energy dissipated by plastic flow (a) and contact (b) after the end of the first phase of intermittent interactions between the sphere and the cantilever beam (end of the light blue area on Figure 19). The dissipated energies are plotted as a function of the time step h for different number of elements n_{el}.

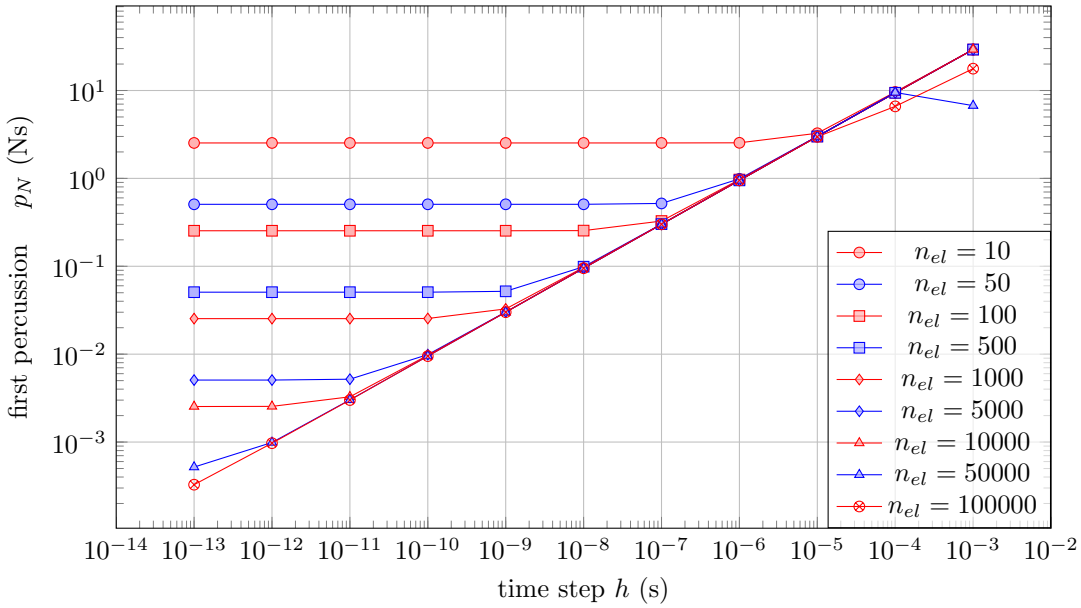

Figure 21: Example 2: First percussion as a function of the time step h when the projectile impacts the free extremity of the cantilever beam.

4.4 Example 3 : Frame made of beams

The last example illustrates the interest of the approach for the analysis of the response of more complex structures subjected to impact, in terms of deformation and energy dissipation.

The chosen structure is a rectangular frame impacted by a projectile (see Figure 22). The frame is 2 meters high and 3 meters large, made of HEB300 in S355 steel (total weigth of 804kg). The structure is clamped at its two extremities. The projectile (mass : $m_p = 1000\text{kg}$) impacts the structure at 0.67m from the ground with a horizontal velocity $v_i = 6\,\text{m/s}$. The characteristics of the structure are summarized in Table 3.

The vertical beams are discretized with 30 elements and the horizontal one with 60 elements. The time step was set at $h = 10^{-5}\text{s}$, which guarantees the accurate approximation of the impact phenomenon and of the structure vibration, as the first natural frequency of the structure is 71Hz. We also set $\theta = 1/2$ to prevent artificial energy dissipation and $e = 0$ to maximize energy dissipation at contact.

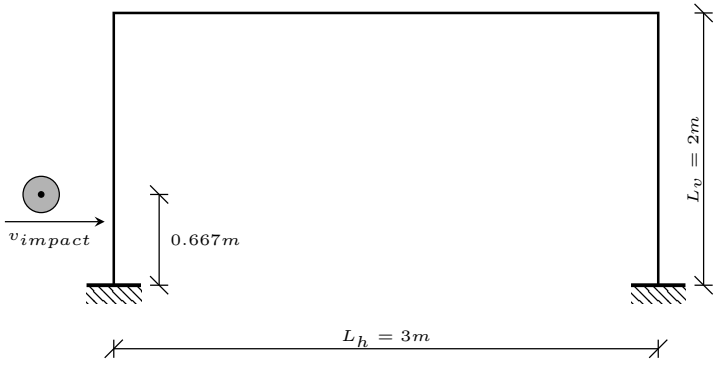

Figure 22: Example 3: Schematic representation of the impacted frame.

A (m^2)	14.9×10^{-3}	I (m^4)	256×10^{-6}
E (MPa)	210 000	ρ ($\mathrm{kg/m}^3$)	7701
n_P (MN)	5.3	m_P (MNm)	0.60
H_{kin} (MPa)	$E/10 = 21\,000$	H_{is} (MPa)	$E/100 = 2100$
$n_{el,v}$	30	$n_{el,h}$	60
m_p (kg)	1000	v_i (m/s)	6

Table 3: Example 3: structure and simulation characteristics.

Influence of elastoplasticity modelling The analysis focused on the influence of the modelling of the material behavior on the energy dissipation and on the plastic strains location, based on comparisons between elasticity, perfect plasticity and plasticity with isotropic and kinematic hardening.

If an elastic material is considered, the impact results in a substantial kinetic energy transfer from the projectile to the structure. After a contact phase lasting around 0.25×10^{-3} s (Figure 23a), the projectile bounces on the structure with a velocity after rebound equal to $-4.24\,\mathrm{m\,s^{-1}}$ (Figure 23b), which corresponds to 71% of the impact velocity. Only a small part of the energy is dissipated at the contact point (1.85% of the impact energy - Figure 24). Consequently, the energy transferred to the structure (48.2% of the impact energy) mainly results in undamped oscillation of the frame.

In the case of perfect plasticity, most of the projectile energy is transferred to the structure and the velocity of the projectile is almost nil after impact ($-0.12\,\mathrm{m\,s^{-1}}$ i.e. 2% of the impact velocity). The impact energy is dissipated by plastic flow in the structure (19.3% of the impact energy) while a large amount results in structure oscillation (79.3% of the impact energy). The energy dissipated at the contact is similar to the energy dissipated for an elastic structure (1.4% of the impact energy).

The integration of hardening only slightly modifies the energy transfers and dissipation compared to perfect plasticity. A slightly smaller amount of energy is dissipated by plastic flow (12.1% of the impact energy) which results in a larger velocity of the projectile after impact $-2.28\,\mathrm{m\,s^{-1}}$, i.e. 38% of the impact velocity). The mechanical energy of the structure after impact and the energy dissipated at the contact (71.9% and 1.5% of the impact energy, respectively) are in the same range as for perfect plasticity.

On the contrary, the locations of the plastic strains in the structure are also significantly different (Figure 25). In the cases of perfect plasticity, local plastic hinges develop near the contact point, the extremities and the connections between beams while, for hardening plasticity, the plastic strains are more broadly distributed around these specific points of the structure. This results seems to be coherent with the results of (Khan, Ahmad, et al., 2021) even if the system is not exactly the same. The creation of plastic hinges for perfect plasticity drastically reduces structure resistance. This may explain the significantly larger duration of the interaction between the structure and the projectile for perfect plasticity (Figure 23b).

Influence of the impact energy Several simulations for increasing values of the impact energy have been done considering either three fixed projectile mass $250\,\mathrm{kg}$, $600\,\mathrm{kg}$ and $1000\,\mathrm{kg}$ and increasing velocities or a fixed impact velocity $4\,\mathrm{m\,s^{-1}}$, $6\,\mathrm{m\,s^{-1}}$ and $8\,\mathrm{m\,s^{-1}}$ and increasing masses. Table 4 shows the values of velocities and masses associated to each kinetic energy level for both cases.

Minor differences in terms of energy dissipation due to plastic flow are observed both for fixed masses and velocities (Figure 26a). More significant differences are observed for the energy dissipated at the contact point (Figure 26b). For increasing velocities and fixed masses, the energy dissipated linearly increases as a function of impact energy with larger increase for larger velocities. On the contrary, for increasing masses, i.e. fixed velocities, the dissipated energy first increases for increasing impact energy and, then, reaches threshold values that are larger for larger impact velocities. This difference is due to the use of a kinematic impact law that depends only on the relative velocities at the impact point and not on the masses of the interacting bodies. Different evolution of the energies dissipated at the contact point could be observed for different impact laws, based on energy restitution coefficient for example.

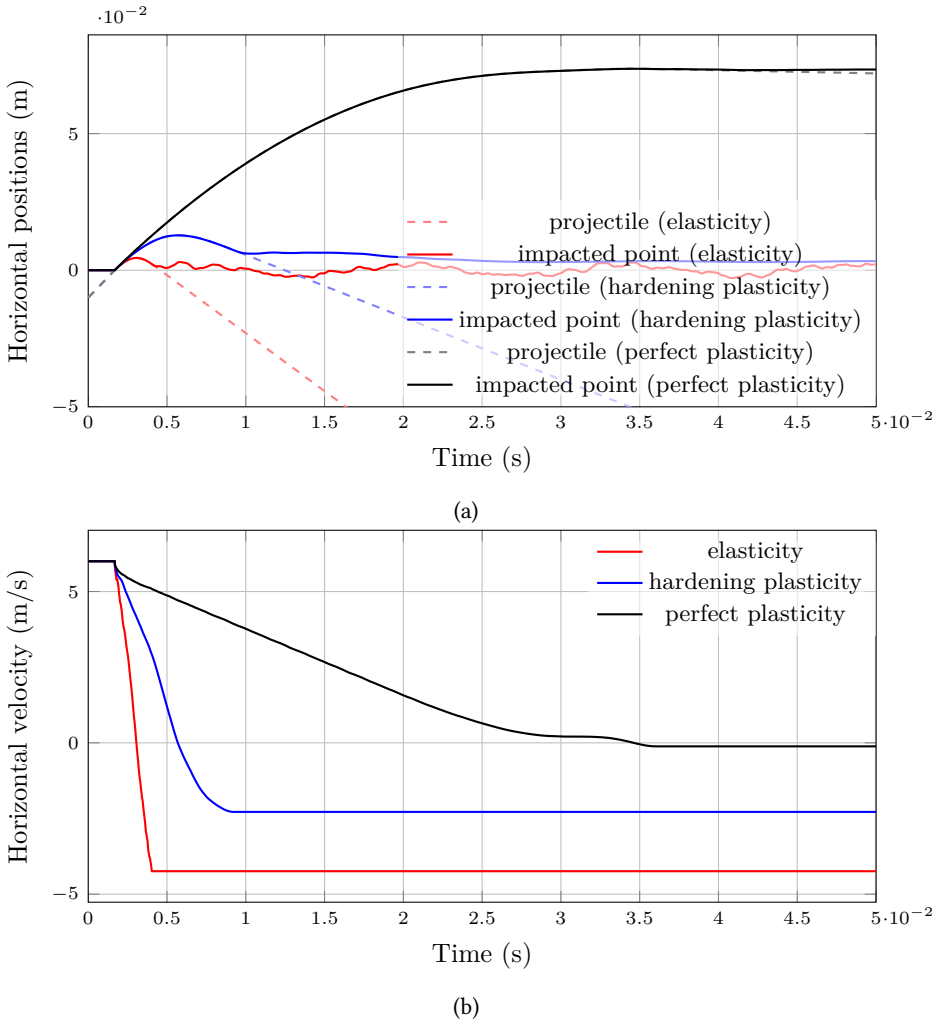

Figure 23: Example 3: Projectile and structure impacted point horizontal positions (a) and projectile velocity (b) as a function of time for different material constitutive and evolution laws (elasticity, perfect plasticity and hardening plasticity).

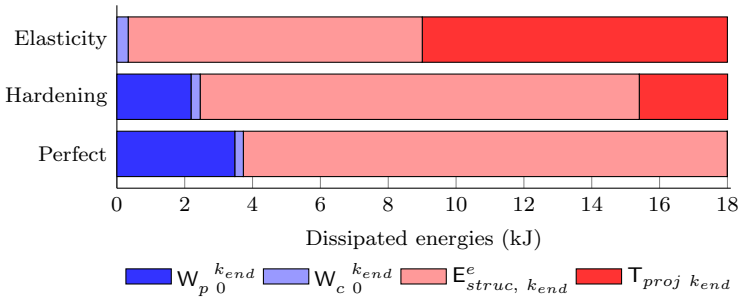

Figure 24: Example 3: Distribution of the initial kinetic energy of the projectile at the end of the simulation. The bar length is the initial projectile energy.

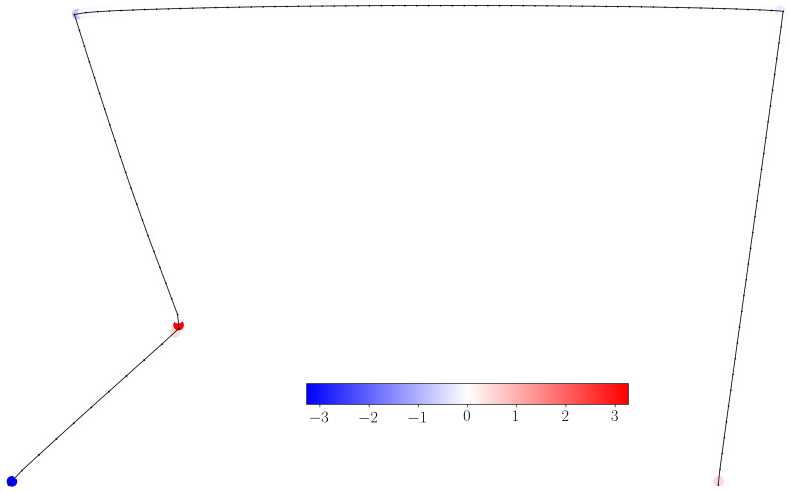

(a) Perfect plasticity

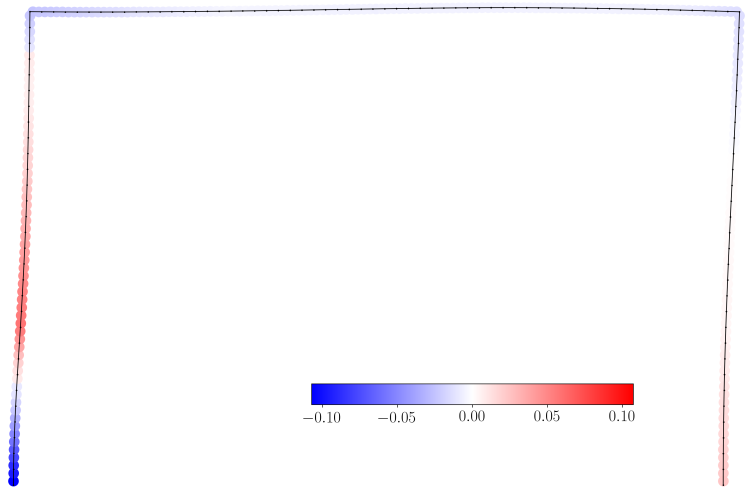

(b) Hardening plasticity

Figure 25: Example 3: Deformed structure 0.0265 seconds after the beginning of the contact (displacements multiplied 100 times) with maximum plastic curvature at each Gauss point.

Impact energy (kJ)	0.5	2	4.5	8	12.5	18	24.5	32
v_i (m/s) ($m_p = 1000$kg)	1	2	3	4	5	6	7	8
v_i (m/s) ($m_p = 600$kg)	1.29	2.58	3.87	5.16	6.45	7.75	9.04	10.33
v_i (m/s) ($m_p = 250$kg)	2	4	6	8	10	12	14	16
m_p (kg) ($v_i = 8$m/s)	15.63	62.5	140.63	250	390.63	562.5	765.63	1000
m_p (kg) ($v_i = 6$m/s)	27.78	111.11	250	444.44	694.44	1000	1361.11	1777.78
m_p (kg) ($v_i = 4$ m/s)	62.5	250	562.5	1000	1562.5	2250	3062.5	4000

Table 4: Example 3: Analysis of the influence of the impact energy on the energy dissipation by plasticity and contact. The impact energy was varied using either fixed masses or fixed velocities. The values of the associated velocities and masses, respectively, are also given.

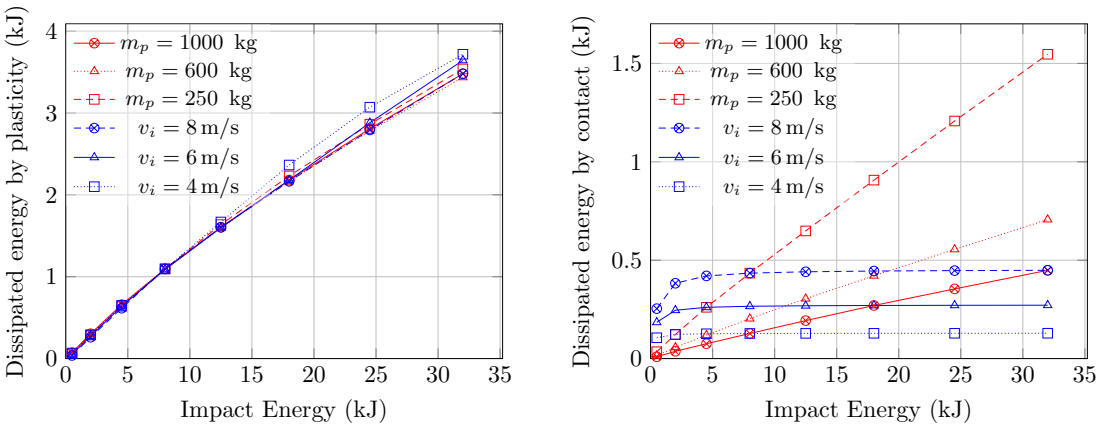

(a) (b)

Figure 26: Energy dissipated by plasticity (a) and by contact (b) in function of the impact energy. The impact energy was varied by using either fixed masses or fixed velocities.

5 Conclusion

This work presents a monolithic algorithm for solving elastoplasticity and contact. The elastoplasticity constitutive and evolution laws are based on the assumption of normal dissipativity formulated as a variational inequality, or equivalently, as a normal cone inclusion. This assumption is also equivalent to the principle of Hill's maximum dissipation, and corresponds to the well-known framework of generalized standard materials. As it is usual in the nonsmooth contact dynamics method, the Signorini contact is also expressed as a variational inequality. Altogether, the dynamics of an elastoplastic system is written as a single variational inequality.

After spatial discretization using a standard iso-parametric finite element method, we end up with a finite-dimensional differential variational inequality that takes into account both the plasticity and the contact constraints. A time–stepping method is developed on the basis of the Moreau-Jean time stepping scheme in order to get a consistent scheme when impact occurs. Especially, some well-posedness results and a discrete energy balance are given which ensure that the scheme is well-posed and stable. The scheme benefits from excellent energy properties under conditions on the θ parameter. For $\theta = 1/2$, the discrete energy balance shows that the numerical dissipation is removed.

The discrete one–step system can be recast into a constrained quadratic optimisation problem which has a unique solution under conditions of positive strain hardening, including perfect plasticity, and a sufficiently small time step. It is then possible to use numerous solving methods for mathematical programming to determine the solution. In particular, if the set of admissible stresses is defined by linear constraints, it is possible to reformulate the quadratic optimisation problem into a monotone Linear Complementarity Problem (LCP).

Finally, numerical examples illustrate the possibilities of the method with the use of the LCP solver to solve elastoplastic dynamical systems with contact without resorting to the return mapping algorithm. The one–step system is solved a the machine accuracy with a single call of a LCP pivoting method. The singular points of the yield function do not raise issues, and the dynamics under impact are validated by the numerical preservation of the energy balance of the system for different configurations.

The framework presented in this paper is general enough to be used in the context of perfect plasticity, or with positive strain hardening in 2D and 3D. The simulation of nonlinear plasticity yield criteria combining several mechanisms should not pose particular problems. The passage into large deformations is one of the objectives of future works as well as the use of different spatial discretization and formulation (Arbitrary Lagrangian-Eulerian (ALE) method, Particle Finite Element Method (PFEM), or Material Point Method (MPM)).

Another perspective is the extension of the proposed approach to non-associated plasticity and Coulomb friction using the Gery De Saxcé (1992) bi-potential approach. This should lead to non-convex optimization problems for which it will be necessary to guarantee the existence of solutions and to find robust nonlinear programming algorithms. Finally, a coupling with cohesive zone models for fracture seems quite simple, based on the recent work of Collins-Craft et al. (2022). The question of softening behaviors is more difficult because it would require using second gradient models or Cosserat media, but this crucial point could deserve a dedicated development.

References

Acary, V. et al. (2011). "A formulation of the linear discrete Coulomb friction problem via convex optimization". In: *ZAMM - Journal of Applied Mathematics and Mechanics / Zeitschrift für Angewandte Mathematik und Mechanik* 91.2, pp. 155–175. ISSN: 1521-4001. [DOI], [HAL].

Acary, Vincent (2016). "Energy conservation and dissipation properties of time-integration methods for nonsmooth elastodynamics with contact". In: *ZAMM - Journal of Applied Mathematics and Mechanics / Zeitschrift für Angewandte Mathematik und Mechanik* 96.5, pp. 585–603. eprint: https://onlinelibrary.wiley.com/doi/pdf/10.1002/zamm.201400231. [DOI], [ARXIV].

Acary, Vincent, Olivier Bonnefon, et al. (Nov. 26, 2019). *An Introduction to Siconos*. (Visited on 06/07/2022).

Acary, Vincent and Bernard Brogliato (Jan. 30, 2008). *Numerical Methods for Nonsmooth Dynamical Systems: Applications in Mechanics and Electronics*. Springer. 529 pp. ISBN: 978-3-540-75392-6.

Bathe, K.J. (1996). *Finite Element Procedures*. Second. Englewood Cliffs, New Jersey: Prentice-Hall.
Belgacem, F.B., P. Hild, and P. Laborde (1998). "The mortar finite element method for contact problems". In: *Mathematical and Computer Modelling* 28.4-8. Recent Advances in Contact Mechanics, pp. 263–271. ISSN: 0895-7177. [DOI], [OA].
Berga, Abdelmajid and Géry De Saxcé (1994). "Elastoplastic finite element analysis of soil problems with implicit standard material constitutive laws". In: *Revue Européenne des Éléments Finis* 3.3, pp. 411–456. [DOI].
Bertrand, D. et al. (2012). "Full-Scale Dynamic Analysis of an Innovative Rockfall Fence Under Impact Using the Discrete Element Method: From the Local Scale to the Structure Scale". In: *Rock Mechanics and Rock Engineering* 45.5, pp. 885–900. ISSN: 1434-453X. [DOI].
Bisbos, C. D., A. Makrodimopoulos, and P. M. Pardalos (Feb. 1, 2005). "Second-Order Cone Programming Approaches to Static Shakedown Analysis in Steel Plasticity". In: *Optimization Methods and Software* 20.1, pp. 25–52. ISSN: 1055-6788. (Visited on 09/27/2021). [DOI].
Bonnans, Joseph-Frédéric et al. (2006). *Numerical optimization: theoretical and practical aspects*. Springer Science & Business Media.
Boyd, Stephen and Lieven Vandenberghe (2004). *Convex optimization*. Cambridge University Press. [DOI].
Bruno, Hugo et al. (2020). "Return-mapping algorithms for associative isotropic hardening plasticity using conic optimization". In: *Applied Mathematical Modelling* 78, pp. 724–748. ISSN: 0307-904X. [DOI].
Capurso, M. (Apr. 1, 1975). "Extended Displacement Bound Theorems for Continua Subjected to Dynamic Loading". In: *Journal of the Mechanics and Physics of Solids* 23.2, pp. 113–122. ISSN: 0022-5096. (Visited on 09/30/2021). [DOI].
Capurso, Michele and Giulio Maier (June 1, 1970). "Incremental Elastoplastic Analysis and Quadratic Optimization". In: *Meccanica* 5.2, pp. 107–116. ISSN: 1572-9648. (Visited on 09/24/2021). [DOI].
Chatterjee, Anindya (May 5, 2004). "The Short-Time Impulse Response of Euler-Bernoulli Beams". In: *Journal of Applied Mechanics* 71.2, pp. 208–218. ISSN: 0021-8936. (Visited on 08/28/2022). [DOI].
Chen, Lin, Hao Wu, and Tao Liu (2021). "Vehicle Collision with Bridge Piers: A State-of-the-Art Review". In: *Advances in Structural Engineering* 24.2, pp. 385–400. ISSN: 1369-4332. [DOI].
Cheng, Long et al. (2015). "A bipotential-based limit analysis and homogenization of ductile porous materials with non-associated Drucker–Prager matrix". In: *Journal of the Mechanics and Physics of Solids* 77, pp. 1–26. ISSN: 0022-5096. [DOI], [HAL].
Christensen, Peter W. (2002a). "A nonsmooth Newton method for elastoplastic problems". In: *Computer Methods in Applied Mechanics and Engineering* 191.11-12, pp. 1189–1219. [DOI].
— (2002b). "A semi-smooth Newton method for elasto-plastic contact problems". In: *International Journal of Solids and Structures* 39.8, pp. 2323–2341. [DOI].
Chrysochoos, A. et al. (1989). "Plastic and dissipated work and stored energy". In: *Nuclear Engineering and Design* 114.3, pp. 323–333. [DOI], [HAL].
Collins-Craft, N.A., F. Bourrier, and V. Acary (2022). "On the formulation and implementation of extrinsic cohesive zone models with contact". In: *Computer Methods in Applied Mechanics and Engineering* 400, p. 115545. [DOI], [HAL].
Corradi, L. (Apr. 1, 1976). "Mathematical Programming Methods for Displacement Bounds in Elasto-Plastic Dynamics". In: *Nuclear Engineering and Design* 37.1, pp. 161–177. ISSN: 0029-5493. (Visited on 09/27/2021). [DOI].
— (1990a). "Finite Element Modelling of the Elastic-Plastic Problem". In: *Mathematical Programming Methods in Structural Plasticity*. CISM International Centre for Mechanical Sciences. 978-3-211-82191-6: Springer Vienna, pp. 255–291. ISBN: 978-3-211-82191-6. [DOI].
— (1990b). "Variational Statements and Mathematical Programming Formulations in Elastic-Plastic Analysis". In: *Mathematical Programming Methods in Structural Plasticity*. CISM International Centre for Mechanical Sciences. 978-3-211-82191-6: Springer Vienna, pp. 231–253. ISBN: 978-3-211-82191-6. [DOI].
Corradi, Leone (1985). "Finite-element formulation of some extremum theorems of incremental plasticity". In: *Engineering Fracture Mechanics* 21.4, pp. 807–816. [DOI].
Corradi, Leone, Osvaldo De Donato, and Giulio Maier (Sept. 1, 1974). "Inelastic Analysis of Reinforced Concrete Frames". In: *Journal of the Structural Division* 100.9, pp. 1925–1942. (Visited on 09/30/2021). [DOI].

Corradi, Leone and Roberto Nova (1974). "A Comparative Study of Bounding Techniques in Dynamic Shakedown of Elasto-Plastic Structures". In: *Earthquake Engineering & Structural Dynamics* 3.2, pp. 139–155. ISSN: 1096-9845. (Visited on 09/30/2021). [DOI].

Davison, Lee (2008). *Fundamentals of shock wave propagation in solids*. Springer Berlin Heidelberg. [DOI], [OA].

De Donato, Osvaldo and Alberto Franchi (May 1, 1973). "A Modified Gradient Method for Finite Element Elastoplastic Analysis by Quadratic Programming". In: *Computer Methods in Applied Mechanics and Engineering* 2.2, pp. 107–131. ISSN: 0045-7825. (Visited on 09/30/2021). [DOI].

De Saxcé, Gery (Jan. 1, 1992). "Une Generalisation de l"inegalite de Fenchel et Ses Applications Aux Lois Constitutives". In: *C.R. Acad. Sci. Paris* 314.

Di Giacinto, Danilo et al. (2020). "A Novel Steel Damping System for Rockfall Protection Galleries". In: *Journal of Constructional Steel Research* 175, p. 106360. ISSN: 0143-974X. [DOI].

Donato, O. de and G. Maier (1972). "Mathematical Programming Methods for the Inelastic Analysis of Reinforced Concrete Frames Allowing for Limited Rotation Capacity". In: *International Journal for Numerical Methods in Engineering* 7.1, pp. 42–43. ISSN: 1097-0207. (Visited on 09/30/2021). [DOI].

Duan, Lian and Wai-Fah Chen (Apr. 1, 1990). "A Yield Surface Equation for Doubly Symmetrical Sections". In: *Engineering Structures* 12.2, pp. 114–119. ISSN: 0141-0296. (Visited on 02/07/2022). [DOI].

Dubois, Frédéric, Vincent Acary, and Michel Jean (2018). "The Contact Dynamics method: A nonsmooth story". In: *Comptes Rendus Mécanique* 346.3, pp. 247–262. [DOI], [OA].

Dupire, S. et al. (2016a). "Novel Quantitative Indicators to Characterize the Protective Effect of Mountain Forests against Rockfall". In: *Ecological Indicators* 67, pp. 98–107. ISSN: 1470-160X. [DOI], [HAL].

— (2016b). "The protective effect of forests against rockfalls across the French Alps: Influence of forest diversity". In: *Forest Ecology and Management* 382, pp. 269–279. [DOI], [HAL].

Facchinei, F. and J. S. Pang (2003). *Finite-dimensional Variational Inequalities and Complementarity Problems*. Vol. I & II. Springer Series in Operations Research. Springer New York. [DOI], [OA].

Germain, P. and E.H. Lee (1973). "On shock waves in elastic-plastic solids". In: *Journal of the Mechanics and Physics of Solids* 21.6, pp. 359–382. ISSN: 0022-5096. [DOI].

Guo, Xuan, Chen Zhang, and ZhiQiang Chen (2020). "Dynamic Performance and Damage Evaluation of a Scoured Double-Pylon Cable-Stayed Bridge under Ship Impact". In: *Engineering Structures* 216, p. 110772. ISSN: 0141-0296. [DOI].

Gurtin, Morton E., William O. Williams, and William P. Ziemer (1987). "Geometric measure theory and the axioms of continuum thermodynamics". In: *Analysis and Thermomechanics*. Springer Berlin Heidelberg, pp. 379–400. [DOI].

Halphen, Bernard and Quoc Son Nguyen (1975). "Sur les matériaux standard généralisés". In: *Journal de Mécanique* 14, pp. 39–63.

Heng, Kai et al. (2022). "Vehicular impact resistance of highway bridge with seismically-designed UHPC pier". In: *Engineering Structures* 252, p. 113635. [DOI].

Heng, Piseth et al. (2016). "A Simplified Model for Nonlinear Dynamic Analysis of Steel Column Subjected to Impact". In: *International Journal of Non-Linear Mechanics* 86, pp. 37–54. ISSN: 0020-7462. [DOI].

— (2017). "An Enhanced SDOF Model to Predict the Behaviour of a Steel Column Impacted by a Rigid Body". In: *Engineering Structures* 152, pp. 771–789. ISSN: 0141-0296. [DOI].

Hill, R. (Jan. 1, 1948). "A Variational Principle of Maximum Plastic Work in Classical Plasticity". In: *The Quarterly Journal of Mechanics and Applied Mathematics* 1.1, pp. 18–28. ISSN: 0033-5614. (Visited on 09/24/2021). [DOI].

Hill, Rodney (1950). *The Mathematical Theory of Plasticity*. Oxford University Press. Oxford Classic Texts in the Physical Sciences. Oxford. ISBN: 0-19-850367-9.

Hiriart-Urruty, Jean-Baptiste and Claude Lemaréchal (1993). *Convex Analysis and Minimization Algorithms*. Vol. I and II. Springer Berlin Heidelberg. [DOI], [OA].

Hjiaj, M., J. Fortin, and G. de Saxcé (2003). "A complete stress update algorithm for the non-associated Drucker–Prager model including treatment of the apex". In: *International Journal of Engineering Science* 41.10, pp. 1109–1143. [DOI].

Houlsby, Guy T and Alexander M Puzrin (2007). *Principles of hyperplasticity: an approach to plasticity theory based on thermodynamic principles*. Springer Science & Business Media.

Houlsby, Guy T. (2019). "Frictional Plasticity in a Convex Analytical Setting". en. In: *Open Geomechanics* 1, 3, pp. 1–10. [DOI], [OA].
Jean, M. (July 20, 1999). "The Non-Smooth Contact Dynamics Method". In: *Computer Methods in Applied Mechanics and Engineering* 177.3-4, pp. 235–257. ISSN: 0045-7825. (Visited on 10/28/2021). [DOI], [HAL].
Jean, M. and J. J. Moreau (1987). "Dynamics in the presence of unilateral contacts and dry friction: a numerical approach". In: *Unilateral Problems in Structural Analysis — 2*. Ed. by G. Del Pietro and F. Maceri. Springer Vienna, pp. 151–196. [DOI], [HAL].
— (1992). "Unilaterality and dry friction in the dynamics of rigid body collections". In: *1st Contact Mechanics International Symposium*, pp. 31–48.
Johnson, K. L. (1985). *Contact mechanics*. Cambridge University Press. [DOI].
Kaewunruen, Sakdirat, Chayut Ngamkhanong, and Chie Hong Lim (2018). "Damage and Failure Modes of Railway Prestressed Concrete Sleepers with Holes/Web Openings Subject to Impact Loading Conditions". In: *Engineering Structures* 176, pp. 840–848. ISSN: 0141-0296. [DOI], [OA].
Kanno, Yoshihiro (Dec. 1, 2016). "A Fast First-Order Optimization Approach to Elastoplastic Analysis of Skeletal Structures". In: *Optimization and Engineering* 17.4, pp. 861–896. ISSN: 1573-2924. (Visited on 10/27/2021). [DOI], [ARXIV].
— (2020). "A note on a family of proximal gradient methods for quasi-static incremental problems in elastoplastic analysis". In: *Theoretical and Applied Mechanics Letters* 10.5, pp. 315–320. [DOI], [OA].
Khan, Azam, Irshad Ahmad, et al. (Nov. 1, 2021). "A Modified Lemke Algorithm for Dynamic Rigid Plastic Response of Skeletal Structures". In: *Computers & Structures* 256, p. 106638. ISSN: 0045-7949. (Visited on 10/12/2021). [DOI].
Khan, Azam, David Lloyd Smith, and Bassam A Izzuddin (May 1, 2013). "Investigation of Rigid-Plastic Beams Subjected to Impact Using Linear Complementarity". In: *Engineering Structures*. Engineering Structures: Modelling and Computations (Special Issue IASS-IACM 2012) 50, pp. 137–148. ISSN: 0141-0296. (Visited on 10/12/2021). [DOI].
Krabbenhøft, K., A.V. Lyamin, and S.W. Sloan (Mar. 1, 2007). "Formulation and Solution of Some Plasticity Problems as Conic Programs". In: *International Journal of Solids and Structures* 44.5, pp. 1533–1549. ISSN: 0020-7683. (Visited on 09/22/2021). [DOI], [OA].
Krabbenhoft, K. et al. (2007). "An interior-point algorithm for elastoplasticity". In: *International Journal for Numerical Methods in Engineering* 69.3, pp. 592–626. [DOI].
Krabbenhoft, Kristian et al. (2005). "A new discontinuous upper bound limit analysis formulation". In: *International Journal for Numerical Methods in Engineering* 63.7, pp. 1069–1088. [DOI].
Langlade, T. et al. (2021). "Modelling of Earthquake-Induced Pounding between Adjacent Structures with a Non-Smooth Contact Dynamics Method". In: *Engineering Structures* 241, p. 112426. ISSN: 0141-0296. [DOI].
Lebeau, G and M Schatzman (1984). "A wave problem in a half-space with a unilateral constraint at the boundary". In: *Journal of Differential Equations* 53.3, pp. 309–361. [DOI], [OA].
Lee, Erastus H. and David T. Liu (1964). "An Example of the Influence of Yield on High Pressure Wave Propagation". In: *Stress Waves in Anelastic Solids*. Springer Berlin Heidelberg, pp. 239–254. [DOI].
Levers, Andrew and Alan Prior (1998). "Finite element analysis of shot peening". In: *Journal of Materials Processing Technology* 80-81, pp. 304–308. [DOI].
Maier, G. (Jan. 1, 1984). "Mathematical Programming Applications to Structural Mechanics: Some Introductory Thoughts". In: *Engineering Structures* 6.1, pp. 2–6. ISSN: 0141-0296. (Visited on 09/23/2021). [DOI].
Maier, G., C. Comi, and A. Corigliano (1991). "Extremum Properties of Finite-Step Solutions in Elastoplasticity with Nonlinear Mixed Hardening". In: pp. 99–102. [DOI].
Maier, G. and E. Vitiello (1974). "Bounds to Plastic Strains and Displacements in Dynamic Shakedown of Work-Hardening Structures". In: *Journal of Applied Mechanics* 41.2, pp. 434–440. [DOI], [OA].
Maier, Giulio (June 1, 1968a). "A Quadratic Programming Approach for Certain Classes of Non Linear Structural Problems". In: *Meccanica* 3.2, pp. 121–130. ISSN: 1572-9648. (Visited on 09/29/2021). [DOI].
— (Dec. 1, 1968b). "Quadratic Programming and Theory of Elastic-Perfectly Plastic Structures". In: *Meccanica* 3.4, pp. 265–273. ISSN: 1572-9648. (Visited on 09/29/2021). [DOI].

Maier, Giulio (Sept. 1, 1969). "Shakedown Theory in Perfect Elastoplasticity with Associated and Nonassociated Flow-Laws: A Finite Element, Linear Programming Approach". In: *Meccanica* 4.3, pp. 250–260. ISSN: 1572-9648. (Visited on 09/29/2021). [DOI].

Maier, Giulio and Leone Corradi (Mar. 1, 1974). "Upper Bounds on Dynamic Deformations of Elastoplastic Continua". In: *Meccanica* 9.1, pp. 30–35. ISSN: 1572-9648. (Visited on 09/30/2021). [DOI].

Majzoobi, G.H., R. Azizi, and A. Alavi Nia (2005). "A three-dimensional simulation of shot peening process using multiple shot impacts". In: *Journal of Materials Processing Technology* 164-165, pp. 1226–1234. [DOI].

Makrodimopoulos, Athanasios and Chris Martin (Jan. 1, 2005a). "A Novel Formulation of Upper Bound Limit Analysis as a Second-Order Cone Programming Problem". In.

— (Jan. 1, 2005b). "Limit Analysis Using Large-Scale SOCP Optimization". In.

Mandel, Jean (1964). "Propagation des surfaces de discontinuité dans un milieu élastoplastique". In: *Stress Waves in Anelastic Solids*. Springer Berlin Heidelberg, pp. 331–340. [DOI].

Maugin, Gerard A (1992). *The thermomechanics of plasticity and fracture*. Vol. 7. Cambridge University Press.

Meng, Jingjing et al. (2020). "A smoothed finite element method using second-order cone programming". In: *Computers and Geotechnics* 123, p. 103547. ISSN: 0266-352X. [DOI].

Moreau, J. J. (1970). "Sur les lois de frottement, de plasticité et de viscosité". In: *Comptes rendus de l'Académie des sciences. Série A - Sciences mathématiques* 271, pp. 608–611.

— (1971). *Fonctions de Résistance et Fonctions de Dissipation*. (Visited on 09/24/2021).

— (1976). "Applications of convex analysis to the treatment of elasto-plastic systems". In: *Applications of Methods of Functional Analysis to Problems in Mechanics*. Ed. by P. Germain and B. Nayroles. Vol. 503. Lecture Notes in Mathematics. Springer Berlin Heidelberg, pp. 56–89. [DOI].

— (1986). "Une formulation du contact à frottement sec; application au calcul numérique". In: *Comptes rendus de l'Académie des sciences. Série 2, Mécanique, Physique, Chimie, Sciences de l'univers, Sciences de la Terre* 302.13, pp. 799–801. ISSN: 0764-4450.

— (1988). "Bounded Variation in Time". In: *Topics in Nonsmooth Mechanics*. Ed. by J. J. Moreau, P.D. Panagiotopoulos, and G. Strang. Basel: Birkhäuser, pp. 1–74.

— (1988). "Unilateral contact and dry friction in finite freedom dynamics". In: *Nonsmooth Mechanics and Applications*. Ed. by J.J. Moreau and Panagiotopoulos P.D. CISM, Courses and lectures 302. Formulation mathematiques tire du livre Contacts mechanics. Wien- New York: Springer Vienna, pp. 1–82. [DOI], [HAL].

Moreau, Jean Jacques (1974). "On unilateral constraints, friction and plasticity". In: *New Variational Techniques in Mathematical Physics*. Ed. by G. Capriz and G. Stampacchia. Springer Berlin Heidelberg, pp. 171–322. [DOI], [HAL].

Musesti, Alessandro (2001). "Balance laws in Continuum Mechanics: a measure-theoretical approach". PhD thesis.

Nguyen, Quoc Son (2000). *Stability and Nonlinear Solid Mechanics*. Wiley, 416 pages.

Nodargi, Nicola A. (2019). "An overview of mixed finite elements for the analysis of inelastic bidimensional structures". In: *Archives of Computational Methods in Engineering* 26.4, pp. 1117–1151. [DOI], [ARXIV].

Nouguier-Lehon, C. et al. (2013). "Surface impact analysis in shot peening process". In: *Wear* 302.1-2, pp. 1058–1063. [DOI].

Parikh, Neal (2014). "Proximal algorithms". In: *Foundations and Trends® in Optimization* 1.3, pp. 127–239. [DOI].

Pellegrino, S. (1993). "Structural computations with the singular value decomposition of the equilibrium matrix". In: *International Journal of Solids and Structures* 30.21, pp. 3025–3035. ISSN: 0020-7683. [DOI].

Popp, Alexander, Michael W. Gee, and Wolfgang A. Wall (2009). "A finite deformation mortar contact formulation using a primal–dual active set strategy". In: *International Journal for Numerical Methods in Engineering* 79.11, pp. 1354–1391. [DOI].

Scherzinger, W.M. (2017). "A return mapping algorithm for isotropic and anisotropic plasticity models using a line search method". In: *Computer Methods in Applied Mechanics and Engineering* 317, pp. 526–553. [DOI], [OA].

Sha, Yanyan, Jørgen Amdahl, and Cato Dørum (2021). "Numerical and Analytical Studies of Ship Deckhouse Impact with Steel and RC Bridge Girders". In: *Engineering Structures* 234, p. 111868. ISSN: 0141-0296. [DOI], [OA].

Shimizu, Wataru and Yoshihiro Kanno (2018). "Accelerated proximal gradient method for elastoplastic analysis with von Mises yield criterion". In: *Japan Journal of Industrial and Applied Mathematics* 35.1, pp. 1–32. [DOI].

— (2020). "A note on accelerated proximal gradient method for elastoplastic analysis with Tresca yield criterion". In: *Journal of the Operations Research Society of Japan* 63.3, pp. 78–92. [DOI], [OA].

Simo, J. C. and T. J. R. Hughes (1998). *Computational Inelasticity*. Springer-Verlag. 405 pp. ISBN: 978-0-387-22763-4. Google Books: EILbBwAAQBAJ. [DOI], [OA].

Son, Nguyen Quoc (1977). "On the elastic-plastic initial-boundary value problem and its numerical integration". In: *International Journal for Numerical Methods in Engineering* 11.5, pp. 817–832. [DOI].

Tangaramvong, S., F. Tin-Loi, and Ch. Song (2012). "A Direct Complementarity Approach for the Elastoplastic Analysis of Plane Stress and Plane Strain Structures". In: *International Journal for Numerical Methods in Engineering* 90.7, pp. 838–866. ISSN: 1097-0207. (Visited on 10/27/2021). [DOI].

Wieners, C. (2007). "Nonlinear solution methods for infinitesimal perfect plasticity". In: *ZAMM* 87.8-9, pp. 643–660. eprint: https://onlinelibrary.wiley.com/doi/pdf/10.1002/zamm.200610339. [DOI], [OA].

Wilkins, Mark L (1963). *Calculation of elastic-plastic flow*. Tech. rep. California Univ Livermore Radiation Lab.

Wright, Stephen J. (1996). *Primal-Dual Interior–Point Methods*. Philadelphia: Society for Industrial and Applied Mathematics. [DOI].

Zeng, Qing, Charikleia D. Stoura, and Elias G. Dimitrakopoulos (2018). "A Localized Lagrange Multipliers Approach for the Problem of Vehicle-Bridge-Interaction". In: *Engineering Structures* 168, pp. 82–92. ISSN: 0141-0296. [DOI].

Zhang, X. et al. (2013). "Particle finite element analysis of large deformation and granular flow problems". In: *Computers and Geotechnics* 54, pp. 133–142. [DOI].

Zhang, Xue (2014). "Particle finite element method in geomechanics". PhD thesis. University of Newcastle Australia.

Zhang, Xue, Kristian Krabbenhoft, et al. (2015). "Numerical simulation of a flow-like landslide using the particle finite element method". In: *Computational Mechanics* 55.1, pp. 167–177. [DOI].

Zhang, Xue, Daichao Sheng, et al. (2017). "Lagrangian modelling of large deformation induced by progressive failure of sensitive clays with elastoviscoplasticity". In: *International Journal for Numerical Methods in Engineering* 112.8, pp. 963–989. [DOI], [HAL].

Zhao, Rong et al. (2022). "A sequential linear complementarity problem for multisurface plasticity". In: *Applied Mathematical Modelling* 103, pp. 557–579. ISSN: 0307-904X. [DOI].

Zheng, Hong, Tan Zhang, and Qiusheng Wang (2020). "The mixed complementarity problem arising from non-associative plasticity with non-smooth yield surfaces". In: *Computer Methods in Applied Mechanics and Engineering* 361, p. 112756. ISSN: 0045-7825. [DOI].

Zhou, Xi-Wen et al. (2023). "A mixed selective edge-based smoothed PFEM with second-order cone programming for geotechnical large deformation analysis". In: *Computers and Geotechnics* 153, p. 105047. ISSN: 0266-352X. [DOI], [OA].

Ziegler, Hans (Mar. 1, 1958). "An Attempt to Generalize Onsager's Principle, and Its Significance for Rheological Problems". In: *Zeitschrift für angewandte Mathematik und Physik ZAMP* 9.5-6, pp. 748–763. ISSN: 1420-9039. (Visited on 09/28/2021). [DOI].

— (1962). *Some Extremum Principles in Irreversible Thermodynamics, with Application to Continuum Mechanics*. Swiss Federal Institute of Technology. 242 pp. Google Books: Bn8LHQAACAAJ.

A Discrete equilibrium matrix

The evaluation of the internal forces using the Gauss quadrature rule is

$$f_{\mathrm{int},e} = \sum_{g=1}^{n_{e,g}} \omega_g B_e^\top(x_g)\sigma_e(x_g) = \sum_{g=1}^{n_{e,g}} \sqrt{\omega_{e,g}} B_e^\top(x_g)\sqrt{\omega_{e,g}}\sigma_e(x_g) \tag{128}$$

where $x_{e,g} \in \mathbb{R}^d, g \in [\![1, n_{e,g}]\!]$ denotes the Gauss points associated their weights $w_{e,g}$ that are positive. Using the standard Gauss quadrature rule, the strain is also evaluated at the Gauss points. We define the notation

$$\varepsilon_{e,g} = B_{e,g}u, \quad \text{with } \varepsilon_{e,g} = \varepsilon_e(x_g) \text{ and } B_{e,g} = B_e(x_g) \tag{129}$$

The strains at Gauss points in an element and in the structure are collected scaled by their weights as follows

$$\varepsilon_e = \mathrm{col}(\sqrt{w_{e,g}}\varepsilon_{e,g}, g \in [\![1, n_{e,g}]\!]) \quad \text{and } \varepsilon = \mathrm{col}(\varepsilon_e, e \in [\![1, n_{\mathrm{el}}]\!]) \tag{130}$$

and, doing in the same way for the matrix $B_{e,g}$, we get

$$\varepsilon_e = B_e u \text{ and } \varepsilon = Bu, \tag{131}$$

with

$$B_e = \mathrm{col}(\sqrt{w_{e,g}}B_{e,g}, g \in [\![1, n_{e,g}]\!]) \quad \text{and } B = \mathrm{col}(B_e, e \in [\![1, n_{\mathrm{el}}]\!]). \tag{132}$$

In the same way, the stresses, evaluated at Gauss points of an element are gathered as follows

$$\sigma_{e,g} = \sigma_e(x_g), \quad \sigma_e = \mathrm{col}(\sqrt{w_{e,g}}\sigma_{e,g}, g \in [\![1, n_{e,g}]\!]) \quad \text{and } \sigma = \mathrm{col}(\sigma_e, e \in [\![1, n_{\mathrm{el}}]\!]) \tag{133}$$

The matrix B appears as the discrete divergence operator, also called the equilibrium matrix in the classical force method.

B Finite element matrices

The elementary form function matrix is

$$\bar{N}_e = \begin{bmatrix} \frac{\xi}{2}(\xi-1) & 0 & 0 & 1-\xi^2 & \frac{\xi}{2}(\xi+1) & 0 & 0 \\ 0 & \frac{1}{4}(1-\xi)^2(2+\xi) & \frac{L_e}{8}(1-\xi)^2(1+\xi) & 0 & 0 & \frac{1}{4}(1+\xi)^2(2-\xi) & -\frac{L_e}{8}(1+\xi)^2(1-\xi) \end{bmatrix} \tag{134}$$

The derivative matrix of N is then:

$$B_e = \begin{bmatrix} \frac{2\xi-1}{L_e} & 0 & 0 & \frac{-4\xi}{L_e} & \frac{2\xi+1}{L_e} & 0 & 0 \\ 0 & \frac{6\xi}{{L_e}^2} & \frac{3\xi-1}{L_e} & 0 & 0 & \frac{-6\xi}{{L_e}^2} & \frac{3\xi+1}{L_e} \end{bmatrix} \tag{135}$$

The elementary consistent mass matrix associated with the element is :

$$M_e = \frac{\rho A L_e}{420} \begin{bmatrix} 56 & 0 & 0 & 28 & -14 & 0 & 0 \\ 0 & 156 & 22L_e & 0 & 0 & 54 & -13L_e \\ 0 & 22L_e & 4{L_e}^2 & 0 & 0 & 13L_e & -3{L_e}^2 \\ 28 & 0 & 0 & 224 & 28 & 0 & 0 \\ -14 & 0 & 0 & 28 & 56 & 0 & 0 \\ 0 & 54L_e & 13L_e & 0 & 0 & 156 & -22L_e \\ 0 & -13L_e & -3{L_e}^2 & 0 & 0 & -22L_e & 4{L_e}^2 \end{bmatrix} \tag{136}$$

where L_e is the element length, A is the cross section area and ρ is the material density.
The elementary elasticity matrix C_e, which relates stresses σ_e and elastic strains ε_e^e, is :

$$C_e = S_e^{-1} = E \begin{bmatrix} A & 0 & 0 & 0 \\ 0 & I & 0 & 0 \\ 0 & 0 & A & 0 \\ 0 & 0 & 0 & I \end{bmatrix} \tag{137}$$

The elementary hardening matrix D_e, which relates internal forces a_e and hardening parameters α_e, is:

$$D_e = \begin{bmatrix} H_{ki}A & 0 & 0 & 0 & 0 & 0 \\ 0 & H_{ki}I & 0 & 0 & 0 & 0 \\ 0 & 0 & H_{is}I & 0 & 0 & 0 \\ 0 & 0 & 0 & H_{ki}A & 0 & 0 \\ 0 & 0 & 0 & 0 & H_{ki}I & 0 \\ 0 & 0 & 0 & 0 & 0 & H_{is}I \end{bmatrix} \tag{138}$$

where H_{ki} and H_{is} are the kinematic and isotropic hardening moduli, respectively.

C Optimality conditions of the problem (76)

In order to derive the optimality conditions for (76), we consider the Lagrangian function

$$\begin{aligned} \mathcal{L}(v, \dot{\varepsilon}, v_{\mathrm{N}}, \sigma, a, \lambda, \mu) \quad = \quad & \frac{1}{2}(v - v_k)^\top M (v - v_k) - \frac{1}{2}(\sigma - \sigma_k)^\top S (\sigma - \sigma_k) - \frac{1}{2}(a - a_k)^\top D^{-1}(a - a_k) \\ & + h\theta \sigma^\top \dot{\varepsilon} - h\theta f_{\mathrm{ext,k+1}}^\top v + \lambda^\top (Bv - \dot{\varepsilon}) + \mu^\top (\theta v_{\mathrm{N}} - H^\top v + (1-\theta) v_{\mathrm{N},k}) \\ & - h\theta \Psi_C \begin{pmatrix} \sigma \\ a \end{pmatrix} + \theta^2 \Psi_{\mathbb{R}^m_+}(v_{\mathrm{N}} + e v_{\mathrm{N},k}). \end{aligned} \tag{139}$$

The optimality conditions of the problem (76) is given by $0 \in \partial \mathcal{L}(v, \dot{\varepsilon}, \sigma, a, v_{\mathrm{N}}, \lambda, \mu)$. Computing the subgradients, we obtain for the optimality conditions

$$\begin{aligned} (\nabla_v \mathcal{L} :) \quad 0 &= M(v - v_k) - h\theta f_{\mathrm{ext,k+1}}^\top + B^\top \lambda - H\mu \\ (\nabla_{\dot{\varepsilon}} \mathcal{L} :) \quad 0 &= h\theta\sigma - \lambda \\ (\partial_\sigma \mathcal{L} :) \quad 0 &\in -S(\sigma - \sigma_k) + h\theta\dot{\varepsilon} - h\theta \partial_\sigma \Psi_C \begin{pmatrix} \sigma \\ a \end{pmatrix} \\ (\partial_a \mathcal{L} :) \quad 0 &\in -D^{-1}(a - a_k) - h\theta \partial_a \Psi_C \begin{pmatrix} \sigma \\ a \end{pmatrix} \\ (\partial_{v_{\mathrm{N}}} \mathcal{L} :) \quad 0 &\in \theta\mu + \theta^2 \partial \Psi(v_{\mathrm{N}} + e v_{\mathrm{N},k}) \\ (\nabla_\lambda \mathcal{L} :) \quad 0 &= Bv - \dot{\varepsilon} \\ (\nabla_\mu \mathcal{L} :) \quad 0 &= \theta v_{\mathrm{N}} - H^\top v + (1-\theta) v_{\mathrm{N},k} \end{aligned} \tag{140}$$

Note that $h\theta\sigma$ appears as the Lagrange multiplier that enforces the condition $Bv = \dot{\varepsilon}$. Introducing the variables z, y, p_{N} such that

$$-\begin{pmatrix} z \\ y \\ p_{\mathrm{N}} \end{pmatrix} \in \partial \Psi_{C \times \mathbb{R}^m_+} \begin{pmatrix} \sigma \\ a \\ v_{\mathrm{N}} + e v_{\mathrm{N},k} \end{pmatrix}, \tag{141}$$

and simplifying the equations, we obtain

$$\begin{cases} M(v - v_k) + h\theta B^\top \sigma = h\theta f^\top_{\text{ext,k+1}} + \theta H p_{\text{N}} \\ S(\sigma - \sigma_k) - h\theta B v = h\theta z \\ D^{-1}(a - a_k) = h\theta y \\ \theta v_{\text{N}} = H^\top v - (1-\theta) v_{\text{N},k} \\ -\begin{pmatrix} z \\ y \\ p_{\text{N}} \end{pmatrix} \in \partial \Psi_{C \times \mathbb{R}^m_+} \begin{pmatrix} \sigma \\ a \\ v_{\text{N}} + e v_{\text{N},k} \end{pmatrix} \end{cases} \tag{142}$$